ANALYSIS OF THE INTERFERENCE BETWEEN ELECTROMAGNETIC ARTICULOGRAPHY AND ELECTROGLOTTOGRAPH SYSTEMS

By

Kelly M. Vonderhaar

A Thesis submitted to the Faculty of the Graduate School, Marquette University, in Partial Fulfillment of the Requirements for the Degree of Master of Science

Milwaukee, Wisconsin

August 2016

ABSTRACT

ANALYSIS OF THE INTERFERENCE BETWEEN ELECTROMAGNETIC ARTICULOGRAPHY AND ELECTROGLOTTOGRAPH SYSTEMS

Kelly M. Vonderhaar, B.S.

Marquette University, 2016

Electromagnetic Articulography (EMA) has become an integral tool for researchers and clinicians who seek to characterize speech kinematics. The position and orientation of the articulators – which include the teeth, lips, and tongue – are recorded by attaching sensors to the articulators and tracking the movement of the sensors through an electromagnetic field. This has been used by researchers and clinicians to better understand dysarthria and synthesize speech, among other applications. Another speech tool, electroglottography (EGG), is used to analyze the movement of the vocal folds during speech production. This is achieved by measuring the time variation of the contact of the vocal folds and analyzing it with regards to the speech produced. Clinically, EGG is used to identify voice abnormalities, including those without visual or acoustic abnormalities.

These systems are not used concurrently because of the electromagnetic field used with the EMA system; NDI and Carstens affirm that metal should be kept out of the field during EMA use. Concurrent use of these systems would lead to simultaneous measurements of the laryngeal and upper airway-articulatory abilities, which could increase understanding of motor speech issues. Parameters derived from the EGG signal could also be incorporated with articulatory parameters to improve synthesized voice quality and synthesize a more realistic voice.

The objective of this research is to investigate whether the interference present between the EMA and EGG systems is significant and, if so, to characterize it so the systems can be used simultaneously. Analysis of the interference was obtained through several data collections. The first assessed the degree of interference when the EMA sensors were stationary. The second data set was collected using a model that maintained sensor orientation while changing the sensors' speed. The final data set was obtained with a model that maintained sensor speed while changing the orientation of the sensors. Sources of interference that were present included the EGG system and orthodontia.

The resulting data led to the conclusion that the presence of the EGG or the orthodontic appliances does not cause significant interference.

ACKNOWLEDGMENTS

Kelly M. Vonderhaar, B.S.

There are so many people that have helped me along the way and who given me the means to achieve more than I could have ever foreseen.

I would like to thank my research advisor, Dr. Michael Johnson, for sharing his time, enthusiasm, humor, and wisdom throughout this entire process. The energy and passion that he devotes to all of his students have been instrumental in my graduate school career, and I will always be thankful for the time that he has dedicated to helping me learn and grow.

I also would like to thank Dr. Jeff Berry, who has been enthusiastic about sharing his knowledge since the beginning and who has devoted a significant amount of time to teaching me how to use the EMA and EGG systems. I am grateful for the knowledge that he has given me and appreciate his problem-solving, especially with regards to the models that were used.

I thank my other lab members, who helped me grow in my own knowledge and who have supported me through this entire process.

I thank my friends and family, who have believed in me from the beginning and who never stopped encouraging me to persevere. Special thanks to my parents and brothers, who have helped me to grow through my college experience and who always support me.

I thank my fiancé Tyler, who has had almost unlimited understanding and patience through the entire writing process and who has encouraged me always.

Finally, I would like to thank my twin brother, Joe, for spending 18 years of education with me. I never would have gotten where I am today without his persistence, intelligence, and humor. Thank you for keeping me going when I wasn’t sure that I would ever be able to finish.

Table of Contents

1. INTRODUCTION 1
1.1 General Background 1
1.2 Research Objective 4
1.3 Thesis Organization 5
2. EMA SYSTEM OVERVIEW 6
2.1 EMA Summary 6
2.2 EMA History 6
2.3 Modern EMA 9
2.4 EMA Orientation Data 11
2.4.1 Quaternion Introduction and Processes 12
2.4.2 Position Data Processing 20
3. EGG SYSTEM OVERVIEW 24
3.1 EGG Summary 24
3.3 EGG Data Post Processing 25
4. INITIAL DETERMINATION OF INTERFERENCE 31
4.1 Methodology 31
4.2 Analysis Methods 33
4.3 Results 34
4.4 Discussion 41
5. DETERMINATION OF EFFECTS OF VELOCITY ON ACCURACY 43
5.1 Purpose 43
5.2 Construction of Model 43
5.3 Baseline Data Collection 46
5.3.1 Methodology 46
5.3.2 Baseline Results 48
5.3.3 Baseline Results Discussion 51
5.4 Analysis with Interference Sources 51
5.4.1 Methodology 51
5.4.2 Results with Interference 53
5.5 Discussion 56
6. DETERMINATION OF EFFECTS OF ORIENTATION ON ACCURACY 59

6.1 Purpose 59
6.2 Construction of Model 59
6.3 Data Collection 61
6.3.1 Methodology 61
6.4 Results 61
6.5 Discussion 65
7. CONCLUSION 68
7.1 Summary 68
7.2 Contributions 70
7.3 Future Work 70
8. REFERENCES 72
9. APPENDICES 74
A. Initial Data Collection 74
B. Lego model 86
C. Lincoln log 92

Table of Figures

Figure 1 - Representation of complex number in complex plane [2] 13
Figure 2 - Calculation of the current sensor norm vector orientation 19
Figure 3 – Axes of the NDI Wave system, with the origin at the center of the field generator [2] 20
Figure 4- Subject with sensors attached to the tongue and lips and a reference sensor on the bridge of the glasses [2] 21
Figure 5 - Biteplate with the MS and OS sensors labeled [2] 22
Figure 6 - Diagram of EGG positioning and use to obtain VFCA measurements [19] 25
Figure 7 - Ideal EGG Waveform segment with the accompanying vocal fold events labeled [20] 26
Figure 8 - Glottal air flow and low frequency component of the EGG signal during an adult male subject's pronunciation of the phrase, "the hut" [19] 28
Figure 9 - Glottal air flow and the high frequency components of the EGG signal during an adult male's pronunciation of the phrase, "the hut" [19] 29
Figure 10 - Data Waveforms from a male subject with F0 at approximately 120Hz. [20] 30
Figure 11 - Biteplate used for stationary trials, with the lowest sensor being sensor 1, the middle sensor being sensor 2, and the highest sensor as sensor 3 31
Figure 12 – Inter-sensor distance biases for sensors 1 and 2 for four interference conditions when sensors are stationary and in center of field 35
Figure 13 – Inter-sensor distance biases for sensors 1 and 2 for four interference conditions when sensors are stationary and are at edge of field 35
Figure 14 – Inter-sensor distance biases sensors 1 and 2 for four interference conditions when sensors are stationary and EGG sensors are outside of the field 36
Figure 15 – Inter-sensor angular biases when the systems were in the center of the field 38
Figure 16 – Inter-sensor angular biases for sensors 1 and 2 in the stationary trials when the systems were at the edge of the field 38
Figure 17 – Inter-sensor angular biases for sensors 1 and 2 in the stationary trials when the EGG sensors were outside of the field 39
Figure 18 – The final Lego model and experimental setup. 45
Figure 19- Path of the sensors on platform of model 46
Figure 20 - Arrangement of the sensors on the non-ferrous rotation model. 47
Figure 21 - Baseline results with the sensors moving at 125.794mm/s. 49
Figure 22 - Moment in which physical jerk occurs 50
Figure 23 - Experimental setup of the non-ferrous rotation model 53
Figure 24 – Inter-sensor distance bias for sensors 6 and 5 in the non-ferrous rotation model under different interference conditions 54
Figure 25 – Inter-sensor angular biases for sensors 6 and 5 in the non-ferrous rotation model with sources of interference present 55
Figure 26 - Construction of the non-ferrous orientation model with palate expander 60
Figure 27 - Diagram of model and its movement 60
Figure 28 – Intser-sensor distance biases for sensors 1 and 2 in the non-ferrous orientation model 62
Figure 29 – Inter-sensor angular biases for sensors 1 and 2 present in the non-ferrous orientation model 64

Figure 30 - Inter-sensor bias for sensors 2 and 3 in stationary trials 74
Figure 31 - Inter-sensor distance bias for sensors 2 and 3 in stationary trials 74
Figure 32 - Inter-sensor distance bias for sensors 2 and 3 in stationary trials 75
Figure 33 - Inter-sensor distance bias for sensors 1 and 3 in stationary trials 77
Figure 34 - Inter-sensor distance bias for sensors 1 and 3 in stationary trials 77
Figure 35 - Inter-sensor distance bias for sensors 1 and 3 in stationary trials 78
Figure 36 – Inter-sensor angular biases present between sensors 2 and 3 in the center of the field for the stationary trials 80
Figure 37 – Inter-sensor angular biases present between sensors 2 and 3 at the edge of the field for the stationary trials 80
Figure 38 - Angular biases present between sensors 2 and 3 with the EGG outside of the field for the stationary trials 81
Figure 39 - Inter-sensor angular biases present between sensors 1 and 3 in the center of the field for the stationary trials 83
Figure 40 - Inter-sensor angular biases present between sensors 1 and 3 at the edge of the field for the stationary trials 83
Figure 41 - Inter-sensor angular biases present between sensors 1 and 3 with the EGG outside of the field for the stationary trials 84
Figure 42 – Distance biases measured with the non-ferrous rotation model while experiencing different sources of interference 86
Figure 43 – Inter-sensor angular bias of the non-ferrous rotation model with sources of interference present 88
Figure 44 - Inter-sensor distances biases for sensors 6 and 5 at approximately 25mm/s in the non-ferrous rotation model 89
Figure 45 - Inter-sensor angular biases for sensors 6 and 5 in the non-ferrous rotation model at approximately 25mm/s 90
Figure 46 - Inter-sensor distance biases for sensors 6 and 5 in the non-ferrous rotation model at approximately 65mm/s 90
Figure 47 - Inter-sensor angular biases for sensors 6 and 5 in the non-ferrous rotation model at approximately 65mm/s 91
Figure 48 - Inter-sensor distance bias for sensors 2 and 3 in the non-ferrous orientation model 92
Figure 49 - Inter-sensor angular bias for sensors 2 and 3 in the non-ferrous orientation model 93
Figure 50 - Inter-sensor distance bias for sensors 1 and 3 in the non-ferrous orientation model 94
Figure 51 - Inter-sensor angular bias for sensors 1 and 3 in the non-ferrous orientation model 95

1. INTRODUCTION

1.1 General Background

Electromagnetic Articulography (EMA) has been developed as an important tool in the characterization of speech kinematics, which can be used in a variety of speech applications that include speech synthesis, speech recognition, and motor learning [1]. In EMA, sensors are attached to the anatomical components of articulation, such as the teeth, lips, and tongue. The subject is then positioned so that his or her head is within an electromagnetic field, and the movements of the sensors are tracked as the subject speaks. The sensors provide information that can be manipulated to obtain the position, velocity, acceleration, and range of motion of the articulators.

Clinically, EMA can potentially increase the accuracy of motor speech disorders. Currently, diagnosis of such disorders occurs mostly through subjective acoustic assessments that are prone to bias from the clinician. The data provided by the EMA can be used to create objective measures that help characterize the degree of the disorder and improve the accuracy and precision of the diagnosis [2].

In the Marquette University Speech and Swallowing Lab, the EMA is currently used in conjunction with the Rehabilitory Articulatory Speech Synthesizer (RASS) system, which uses the position and orientation data provided by the EMA sensors to derive input parameters to a Maeda synthesizer [3]. The virtual vocal tract allows researchers to manually adjust these parameters to study how changing one parameter affects the synthesized voice. Through the use of sensor-to-synthesizer mapping and post-processing software, auditory feedback can be offered to the subject as a method to influence the subject's articulation.

The electroglottograph (EGG) is another system that has been used to characterize speech disorders, specifically of the laryngeal variety. When using the EGG, two electrodes are attached to the throat, one on either side of the vocal folds. A small current is passed between them – as the vocal fold contact area (VFCA) changes with vocal fold vibration, the change in resistance is recorded by the system [4]. The researcher or clinician can then interpret the information to show the area and duration of contact.

The primary clinical use of the EGG is to diagnose patient voice abnormalities and disorders. In two studies conducted by Behrman and Orlikoff, patients with voice abnormalities were assessed and treated successfully using the EGG [5]. One of these patients had no visual or acoustic abnormalities, and it was only with the use of the EGG as both a diagnosis tool and as a measure of the progress made with treatment that the subject regained normal speech [5].

If used together, the EMA and EGG systems could potentially provide useful information both with regards to clinical diagnosis and to research. With regards to RASS, the current configuration uses a generic LF model of glottal flow. The EGG signal contains information such as the fundamental frequency, open quotient, and skewing quotient that could aid the RASS system in producing a more realistic synthesized version of the subject's voice [3]. The objective would be to utilize the EMA and EGG systems simultaneously to allow for real-time updates of the input parameters to the RASS system. As a result, it would be possible to conduct studies involving changes in pitch and vocal quality in addition to the current ability to study vocal tract perturbation [3]. Story also suggested that incorporating laryngeal data with articulator movement data would create a more successful voice synthesizer. He pointed out that the vibration of the

vocal folds generates flow pulses that create acoustic resonances of the nasal passages, trachea, and vocal tract [6]. The movement of the articulators is responsible for shifting the characteristics of the resulting acoustic wave, essentially acting as a modifier of the carrier signal. From this perspective, the development of a synthesis model requires a set of parameters that allows time-dependent control of both the shape of the vocal tract area and the way that it is coupled to the nasal system. However, Story argued that to create a complete model for speech synthesis, it would also be necessary to include kinematic representations of the vocal fold surfaces with the model of the vocal tract area. Using the EGG to obtain data concerning vocal fold contact area while simultaneously collecting data regarding EMA sensor position would allow for a more accurate model. Without simultaneous collection, these parameters can only be understood by collecting first EMA data, then EGG, before attempting to shift the signals so that they align correctly.

With regards to clinical application, using the EMA and EGG systems together would aid in the understanding of dysarthria, which can affect the speech subsystems (respiratory, laryngeal, resonance, and articulatory). Having additional concurrent physiological data would provide a more detailed understanding of the motor problems involved with the different abnormalities and dysphonia.

However, the EGG and EMA systems are currently not used simultaneously. As EMA utilizes an electromagnetic field, the presence of additional metal within the field is hypothesized to create interference with the EMA system and result in inaccurate position and orientation data. EMA system descriptions include warnings about this interference. The Carstens AG500 system, for example, states that the sensors should be positioned so that interference from metal will be minimal [7], and effort has been devoted to

constructing a calibration mechanism that doesn't contain any metal and so won't affect the system [8]. The NDI Wave user's manual states that the field generator should not be in the vicinity of any metal equipment within a radius of 1.0m, with the field generator at the center of the sphere [9].

1.2 Research Objective

The objective of this research is to determine whether there is a significant level of interference between the EGG and EMA systems when used simultaneously. If so, the secondary objective is to characterize the interference and create an algorithm to reduce the interference and allow for simultaneous use of the EGG and EMA Additional trials have been added to examine whether a significant level of interference is present when orthodontic appliances are present. The orientation data provided by the EMA system during these trials has also been analyzed. As the quaternion data used to represent orientations is not familiar to many researchers in the speech and audiology research communities, a brief description of quaternions and their different mathematical operations has been included.

The level of interference was deemed to be significant if the presence of the EGG caused the measurements of the EMA system to exceed the error specification of the system, which, in the Marquette Speech and Swallowing Lab, is the NDI Wave system. This thesis describes the standard deviation in inter-sensor distance and angle measurements with and without sources of interference present and so provides the user with an understanding of the degree to which metallic interference affects EMA sensor measurement data.

1.3 Thesis Organization

This thesis contains seven chapters and an appendix. The second chapter describes the history of EMA systems and provides both a technical understanding of how the EMA systems work and a description of the data that is gathered. The third chapter provides an explanation for how the EGG system works and the method by which the resulting waveform is analyzed. The fourth chapter presents the initial experiments performed to determine if there was interference present in the EMA signal when the EGG was present and the EMA sensors were kept stationary. The fifth chapter elaborates on this analysis by placing the EMA sensors on a moving platform in order to explore the effects of velocity on the EMA results, both with and without the EGG present. Two dental orthodontic appliances were also placed in the field to test the effect of orthodontia on the EMA system results. The sixth chapter describes a similar exploration that was accomplished by putting the EMA sensors along an axis of rotation. The effects of the EGG system and orthodontic devices on the EMA data were assessed to determine the degree of interference. The seventh chapter contains a summary of the previous chapters and explains the implications of the results, particularly in regards to clinical applications in speech pathology. The appendices contain additional figures and tables from the trials that were deemed nonessential to the thesis but that the reader may find useful in further understanding of the conclusions drawn by the thesis.

2. EMA SYSTEM OVERVIEW

2.1 EMA Summary

Electromagnetic articulography is a methodology that enables the tracking of articulator position and orientation during speech. This is accomplished through the attachment of sensors to the articulators. The sensors' kinematic data is then recorded in a 3-D coordinate system as the articulators are moved through an electromagnetic field.

Advantages of using EMA over radiological procedures, such as x-ray microbeam, include increased information concerning the movements of the tongue and lesser radiation for the subject. In addition, the location of the mandibular bone, which can cause a shadow during radiological procedures if the subject is not positioned correctly, is not a factor in EMA [10]. However, changes in orientation often present issues in obtaining accurate data from the sensors, which Perkell et. al. (1992) refers to as an issue of rotational misalignment [10]. This is most likely to be observed with tongue and jaw sensors, which experience a change in orientation with variations in pitch [11].

The NDI Wave system, which is used by the Marquette Speech and Swallowing Lab, has a spatial resolution of less than 0.5 mm. The sampling frequency is 400 Hz, which results in a temporal resolution of 0.0025 s [11].

2.2 EMA History

Developing an accurate method to track the movement and orientation of sensors with regards to speech is valuable for several important applications, such as assembling a database that could establish statistical characterizations of speech movements to aid with dysarthria characterization [12]. For instance, tracking articulator movement can be

used to assess the tongue-jaw coordination during speech for subjects who had suffered a traumatic brain injury (TBI) [13]. An additional application is incorporation of articulator position and orientation data into speech synthesis models; for example, computer-animated talking heads utilize two-dimensional dynamic tongue movement data from articulatory sensors [14]. Due to the variety of applications, it was deemed important to implement a method for tracking articulator movements.

One initial response to this need was the development of x-ray microbeam systems, such as the one described by John R. Westbury [12]. This system determines the location of spherical gold pellets inside its image field by aiming an x-ray beam in the direction of the pellets. Positions are then assigned to each pellet based on the point on the 2D midsagittal plane at which the maximum absorption occurs. The tracking process involves stepping the x-ray beam across the system field in small intervals. The subject is seated between an x-ray detector and an x-ray generator containing a pinhole. Under optimal conditions and with an image plane that is 60 cm from the system pinhole, the pellet centers can be found at spatial intervals separated by a minimum of 0.0625 mm. The spatial resolution is inversely proportional to the distance that lies between the image plane and the system pinhole [12].

However, Westbury also noted several disadvantages of this system [12]. While positional error during dynamic trials was not quantified, it has been hypothesized that the error is velocity-dependent. The pellet might move across an entire grid interval in the time that it takes for the system to produce the raster. The changing sensor position will thus not be correctly perceived by the system. In addition, subjects were exposed to ionizing radiation during the procedure. While steps were taken to limit the exposure,

such as decreasing the dwell-time of the x-ray beam per unit area, this method still put subjects at risk [12].

In order to address these concerns, Perkell et al. introduced the ElectroMagnetic Midsagittal Articulometer (EMMA) system [10]. This system took advantage of alternating magnetic fields to measure motion. The fundamental principle is that when a transmitter coil and a transducer coil are separated by a distance and lie parallel to one another with midlines on the same axis, the flux density is inversely proportional to the cube of the distance from the transmitter. The alternating magnetic field sent through the transducer coil induces an alternating signal, which is proportional to flux linkage and thus proportional to the cross-sectional area of the transducer coil and the flux density. As a result, the voltage induced in the transducer is inversely proportional to the cube of the distance between transmitter and transducer [10].

Three magnetic-field transmitters, driven at different carrier frequencies, are oriented so that they are parallel to one another and perpendicular to the plane established by their sensors. Single-axis transducer coils are fixed to the articulators so that their centers are located within the plane of measurement while the coils themselves are perpendicular to the plane. When the subject speaks, the transducers become misaligned as a result of the tilt and twist. The voltage that each transmitter induced was reduced by a factor of the cosine of the angle of misalignment [10].

While less hazardous than the x-ray microbeam system, the three-transmitter system relied heavily on the accurate placement of the transmitters in the midsagittal plane. Incorrect placement led to rotational misalignment and incorrect position

measurements. Similarly, erroneous measurements would occur if the articulators moved perpendicular to the midsagittal plane [10].

2.3 Modern EMA

In order to solve the issue of rotational misalignment, Zierdt, Hoole, and Tillman created a three-dimensional EMA system [15]. The waves generated by the coils differ from regular radio waves in that they do not interfere with each other or most matter, making it possible for transmitters to be set up in spherical orientation.

The receiver coil can be viewed as a dipole with five degrees of freedom: three Cartesian coordinates and two angles that represent the alignment of the dipole. Each of these values must be found to determine the coil's position. By placing the six transmitter coils in a sphere with a right angle between them, an absolute symmetrical arrangement is achieved [15]. The spherical arrangement results in each receiver coil not being perpendicular to more than three transmitters at any given point. The voltage measured at the receiver coils changes as a function of the varying distance and angle between the axis of each transmitter as well as a function of each sensor. The six voltage amplitudes can then be used to calculate the distance between each transmitter and each sensor. The six transmitter coils provide six equations with which to calculate the values that describe the Cartesian coordinates and angular position of the receiver coil [7]. By creating a three-dimensional system, the data gathered about the sensor increased to include two rotational degrees of freedom. [15]

This principle was used to create the modern Carstens AG500 and AG501 (Carstens Medizinelectronik, Lenglern, Germany) EMA systems, described by Yunusova

et. al. in 2009 [7]. The six transmitter coils are arranged spherically on a plexiglass cube, with each transmitter driven at different frequencies ranging from 7.5 to 13.75 kHz. The receiver coils and subject are positioned inside of this cube while data is collected. The AG500 system is capable of tracking up to 12 sensors simultaneously, with signals acquired at 200 Hz [7].

Another commercial 3D EMA system is the NDI Wave system, which is a proprietary EMA system that contains a data collection unit and a rectangular box containing the transmitter coils [9]. The box with the transmitter coils can be placed around the subject as desired. The standard Wave system allows for an electromagnetic field of either 300 mm^3 or 500 mm^3 at 100 Hz. It is capable of tracking up to eight sensors with an accuracy within 0.5 mm, which falls within the acceptable error for the analysis of speech kinematics [11]. An upgraded unit allows for an increased sampling rate of 400 Hz, and a second data collection unit can be attached to allow for eight more sensors to be used to obtain data [9]. This upgraded NDI Wave system is the EMA unit that is used by the Marquette University Speech and Swallowing Lab. The Wave system requires no user calibration to minimize error, unlike the alternative AG500 system [11].

There are alternative methods of tracking articulator movement besides EMA. One such method is collecting real-time articulatory and acoustic data using a multimodal real-time MRI [16]. While the current sampling rates of rtMRI are lower that of the EMA and the x-ray microbeam systems, midsagittal rtMRI allows for analysis of not just the tongue, lip, and jaw movements, but also of the velum, pharynx, and larynx movements. Subjects are positioned within the MRI scanner and given text to read as their upper airways are imaged. At the same time, the audio signals are collected at a sampling

frequency of 20 kHz using a fiber-optic microphone noise-cancelling system. The internal clock of the MRI is used to help synchronize the acoustic signal with the images.

Another method is combining ultrasound with the Optotrak system [17], which is produced by NDI. Optotrak uses three coupled charge-coupled devices as a way to identify the locations of infra-red-emitting diodes (IREDS) in space. Each IRED is about 5mm in diameter, and can be attached to the lips, chin, and other exterior points. When used with ultrasound, three IREDS are attached to goggles that the subject wears to provide a reference for the position of the ultrasound probe. Three additional IREDs are attached to the handle of the ultrasound probe. An alignment program analyzes the Optotrak data to calculate the position and orientation of the probe relative to the head. The ultrasound component allows users to image the tongue in either sagittal or coronal orientation. However, contact must be made between the skin and probe at all times; this is commonly maintained through either hand-applied pressure or with elastic cords fastened over the head.

2.4 EMA Orientation Data

The Wave system can be utilized to obtain data about each sensor's three-dimensional position. The position of the sensor is given by Cartesian coordinates, which can be used to track the trajectory of the sensor and its distance in regards to the other sensors. The sensors also provide information regarding the orientation of the sensor, which is given in the form of quaternions. The orientation data can be either two-dimensional or three-dimensional, depending on whether the sensors are 5-degrees-of-freedom (5-DOF) or 6-degrees-of-freedom (6-DOF). 5-DOF sensors track the Cartesian spatial coordinates but also track the angular coordinates that describe rotation around

the anterior-posterior axis, also known as roll, and rotation around the transverse axis, also known as pitch. 6-DOF sensors also track these coordinates, but they additionally track the angular coordinates that describe the rotation about the inferior-superior axis, also known as yaw [11]. Orientation data is provided through a four-dimensional quaternion vector that represents the three-dimensional rotation of the sensor relative to an established baseline orientation. Quaternions have generally been used to computer graphics and aviation but have recently become used with regards to speech processing [2]. With this in mind, a brief introduction to quaternions has been included.

2.4.1 Quaternion Introduction and Processes

Quaternions were first formalized in 1843 by Sir William Hamilton in his attempts to generalize complex numbers so that they could be used with respect to three-dimensional space. Since complex numbers have an imaginary component, Hamilton believed that he would have to identify at least one additional imaginary component to achieve his goal. According to a letter that Hamilton wrote to his son Archibald, Hamilton was walking to a meeting of the Royal Irish Academy when the solution to the complex number problem struck him. He carved the solution into the nearby Broome Bridge so that in the event that he forgot or collapsed, his work would not be lost. [18]

Hamilton recognized that quaternions are closely related to three-dimensional rotations, a fact which was first published by Arthur Cayley in 1845. Hamilton also devised a quaternion multiplication rule with three additional rules related to complex multiplication. This multiplication rule further expresses the connection between unit-length, four-dimensional vectors – quaternions – and three dimensional rotations. This

connection was also a conclusion that Olinde Rodrigues arrived at by examining rotation formulas [18].

An initial review of complex numbers will be presented before the quaternion is introduced [2]. A complex number consists of a real component and an imaginary component, such as

$$c = a + b\boldsymbol{i}\,. \tag{2.4.1}$$

The components *a* and *b* are real numbers, and ***i*** is equal to $\sqrt{-1}$. When graphing a complex number, the vertical axis is considered the imaginary axis and the horizontal axis is considered the real axis, as seen below in this plot of $c = 3 + 4\boldsymbol{i}$ [2].

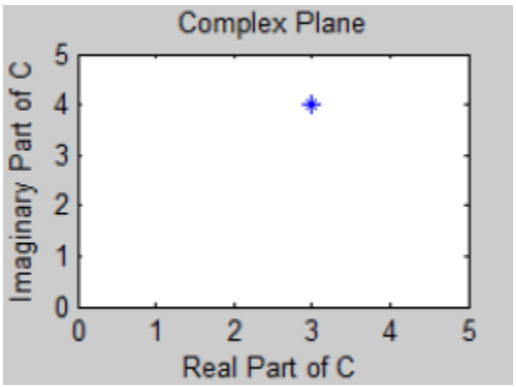

Figure 1 - Representation of complex number in complex plane [2]

Complex addition and subtraction are accomplished by adding or subtracting the real components of the complex numbers and then adding or subtracting the imaginary components of the complex numbers such as

$$(a + b\boldsymbol{i}) + (c + d\boldsymbol{i}) = e + f\boldsymbol{i}\,, \tag{2.4.2}$$

where e is equal to $(a + c)$ and f is equal to $(b + d)$ [2].

The multiplication of complex numbers is distributive, meaning that the order in which the complex numbers are multiplied does not matter:

$$(a+b\boldsymbol{i})(c+d\boldsymbol{i}) = (c+d\boldsymbol{i})(a+b\boldsymbol{i}) = (ac-bd)+(ad+bc)\boldsymbol{i}\,. \tag{2.4.3}$$

The complex conjugate is found by changing the sign of the imaginary part of the complex number:

$$c^{*} = a - b\boldsymbol{i}\,. \tag{2.4.4}$$

In two dimensions, the rotation of a complex number takes place through a rotor. A rotor can be defined as a complex number that is used to rotate another complex number by an angle θ around the origin. The specific rotor can be found through the equation below:

$$r = \cos\theta + \boldsymbol{i}\sin\theta\,. \tag{2.4.5}$$

By multiplying the rotor with the complex number to be rotated, the final rotated complex number can be obtained [2].

A quaternion exists in a four-dimensional space that is comprised of a real axis and three orthogonal imaginary axes, marked as ***i***, ***j***, and ***k***. In general, quaternions can be written with respect to these axes, as in the form seen in the equation below:

$$\boldsymbol{q} = w + x\boldsymbol{i} + y\boldsymbol{j} + z\boldsymbol{k}\,. \tag{2.4.6}$$

In this representation, *w*, *x*, *y*, and *z* are real numbers and satisfy the following equation:

$$\boldsymbol{i}^2 = \boldsymbol{j}^2 = \boldsymbol{k}^2 = \boldsymbol{ijk} = -1. \tag{2.4.7}$$

The above equation shows the parallels that can be drawn between complex numbers quaternions. The primary difference is that quaternions contain two additional imaginary dimensions, which allows for three-dimensional rotation and additional complexity in behavior [2].

Another common notation is that of a real number and a vector, seen below:

$$\boldsymbol{q} = (w, \boldsymbol{v}), \tag{2.4.8}$$

where w is the real component of the quaternion and $\boldsymbol{v}$ is a vector containing the $\boldsymbol{i}$, $\boldsymbol{j}$, and $\boldsymbol{k}$ components with coefficients of x,y,and z respectively.

Unit-normalized quaternions can be used to conceptualize the rotation of complex numbers in three-dimensional planes. Normalizing quaternions is also similar to normalizing vectors, as seen here:

$$norm(\boldsymbol{q}) = \frac{\boldsymbol{q}}{\sqrt{w^2 + x^2 + y^2 + z^2}}. \tag{2.4.9}$$

A normalized quaternion will have a magnitude of one. Normalized quaternions, also known as unit-length quaternions, are desirable for rotations of vectors because the quaternion magnitude of one results in the vector magnitude being unchanged through multiplication [2].

The inverse of a quaternion can be found using a similar method to the normalized quaternion:

$$\boldsymbol{q}^{-1} = \frac{\boldsymbol{q}^{*}}{\sqrt{w^2 + x^2 + y^2 + z^2}}. \tag{2.4.10}$$

If the magnitude of the quaternion is one before the inverse operation is performed, the inverse quaternion will be equal to the conjugate of the quaternion

Rotating a quaternion is similar to the rotation of a complex number. The imaginary components of the quaternion describe the axis about which another point or vector will be rotated. In order to rotate a point by an angle θ in three-dimensional space, the following equation must be used:

$$\boldsymbol{q} = \left[\cos\left(\frac{\theta}{2}\right), \sin\left(\frac{\theta}{2}\right)(x\boldsymbol{i} + y\boldsymbol{j} + z\boldsymbol{k}) \right], \tag{2.4.11}$$

where x, y, and z describe the axis of rotation.

As an example, if a unit vector in the positive x-direction ([1,0,0]) were to be rotated to the y-axis ([0,1,0]), a 90° rotation would be required. The quaternion required to effect this rotation would be equal to

$$\boldsymbol{q} = \left[\cos(\frac{90^\circ}{2}), \sin(\frac{90^\circ}{2})(0\boldsymbol{i} + 0\boldsymbol{j} + 1\boldsymbol{k}) \right]. \tag{2.4.12}$$

The resulting quaternion would be $\boldsymbol{q} = \left[\frac{\sqrt{2}}{2}, \frac{\sqrt{2}}{2}\boldsymbol{k} \right]$. The rotated vector can be calculated using the sandwich product rule seen below:

$$v_{rotated} = \boldsymbol{q}\boldsymbol{v}\boldsymbol{q}^{-1}. \tag{2.4.13}$$

In this equation, $\boldsymbol{q}$ represents the quaternion for the desired rotation, $\boldsymbol{q}^{-1}$ represents the inverse of that quaternion, and $\boldsymbol{v}$ is the vector represented as a pure quaternion. A pure quaternion requires that the vector's *x*, *y*, and *z* components are represented as the $\boldsymbol{i}$, $\boldsymbol{j}$, and $\boldsymbol{k}$ components of the quaternion. [2] Note that since the quaternion is already a unit-

normalized quaternion, the inverse of the quaternion is the same as the conjugate of the quaternion.

The resulting vector becomes

$$v_{rotated} = \left[\frac{\sqrt{2}}{2}, \frac{\sqrt{2}}{2}k\right]\left[0,1i+0j+0k\right]\left[\frac{\sqrt{2}}{2}, -\frac{\sqrt{2}}{2}\right] = \left[0,1,0\right]. \quad (2.4.14)$$

While in this case a 90°-rotation was used, a 270°-rotation in the opposite direction would have achieved the same result. In addition, a different axis of rotation could have been used. This operation was used to rotate between two points and so can be called a point rotation, in which the vector is rotated but the system axes remain stationary. In a frame rotation, which occurs in the equation shown below, the coordinate axes are rotated while the vector remains stationary [2]:

$$v_{rotated} = \boldsymbol{q}^{-1}\boldsymbol{v}\boldsymbol{q}. \quad (2.4.15)$$

Quaternion addition can be carried out using the same method as complex number addition. However, quaternion multiplication differs from complex number multiplication; unlike complex number multiplication, quaternion multiplication is not commutative, meaning that the order of multiplication matters. Quaternion multiplication follows the same rules as those of taking a cross product between vectors, as seen below: [18]

$$\boldsymbol{p}\boldsymbol{q} = \left(p_0, p_1, p_2, p_3\right)(q_0, q_1, q_2, q_3) = \begin{bmatrix} p_0q_0 - p_1q_1 - p_2q_2 - p_3q_3 \\ p_1q_0 + p_0q_1 + p_2q_3 - p_3q_2 \\ p_2q_0 + p_0q_2 + p_3q_1 - p_1q_3 \\ p_3q_0 + p_0q_3 + p_1q_2 - p_2q_1 \end{bmatrix}. \quad (2.4.16)$$

$$= (p_0q_0 - \boldsymbol{p}\boldsymbol{q}, p_0\boldsymbol{q} + q_0\boldsymbol{p} + \boldsymbol{p}\times\boldsymbol{q})$$

Taking the conjugate of a quaternion is similar to taking the conjugate of a two-dimensional complex number. The sign of the imaginary components is reversed to form the conjugate, as seen below: [18]

$$q^* = (w, -\boldsymbol{v}) = w - x\boldsymbol{i} - y\boldsymbol{j} - z\boldsymbol{k} . \tag{2.4.17}$$

These operations can be used to find the difference between two quaternions as a measure of the net angle between them, as follows:

$$diff(\boldsymbol{p}, \boldsymbol{q}) = \boldsymbol{p}^* \boldsymbol{q} , \tag{2.4.18}$$

where the multiplication taking place is the quaternion multiplication seen above in Eq. 2.4.16.

Since quaternion multiplication is not commutative, the difference formula for quaternions is not commutative. In order to calculate the difference between two quaternions, the two quaternions **p** and **q** are first normalized. The two differences $diff(\boldsymbol{p}, \boldsymbol{q})$ and $diff(\boldsymbol{q}, \boldsymbol{p})$ are then calculated using Equation 2.4.18 above. The angle of rotation is calculated from each of these differences using the following equation:

$$theta(\boldsymbol{p}, \boldsymbol{q}) = 2\cos^{-1}\left(diff(\boldsymbol{p}, \boldsymbol{q})\right), \tag{2.4.19}$$

where the inverse cosine is calculated in degrees.

It is desirable for distance measures to be symmetric. Since $theta(\boldsymbol{p}, \boldsymbol{q})$ and $theta(\boldsymbol{q}, \boldsymbol{p})$ are not equivalent values, a symmetric distance measure can be created by averaging the two theta values together in order to calculate the net angle difference between the two quaternions:

$$average = \frac{theta(\boldsymbol{p},\boldsymbol{q}) + theta(\boldsymbol{q},\boldsymbol{p})}{2}. \qquad (2.4.20)$$

With this in mind, the orientation data provided by the EMA sensors can be interpreted more easily. As quaternions represent rotations between two vectors, the quaternion itself does not represent the absolute orientation of the sensor. With regards to the NDI Wave system, quaternions represent the rotation required to acquire the sensor's present orientation from a baseline orientation [2].

Specifically, the quaternion information gathered from the NDI Wave describes the rotation that is needed to rotate a vector that is normal to the XY plane to the current sensor norm vector orientation. The example shown below in uses multiples the vector [0,0,1] by the sensor's quaternion data to obtain the present sensor norm vector orientation [2].

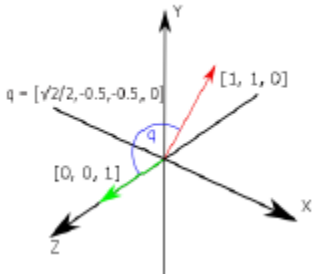

Figure 2 - Calculation of the current sensor norm vector orientation

The [0,01] vector represents the baseline data provided by the NDI Wave system. Multiplying the sensor's quaternion q vector by the baseline data results in the direction shown by the [1,1,0] vector *[2]*.

2.4.2 Position Data Processing

When tracking speech kinematics, it is important to be able to accurately track where the sensors are positioned during the data collection. It is often valuable to transform the data into a new coordinate system for a better understanding of sensor movement. There are several available reference spaces in which EMA Cartesian coordinate data can be presented, including a global coordinate system, a head-corrected space, and a bite-plate-corrected space. Within the global coordinate system, the x,y, and z axes are defined with respect to the field generator box, as seen below in Figure 3. The origin of the axes is found at the center of the box. The x-axis is represented by the red arrow and is oriented vertically, with the positive x-direction pointing upwards. The y-axis is represented by the green arrow and is pointed forward, towards the right side of the transmitter box. The z-axis is oriented into the transmitter and is represented by a blue arrow, unseen here because of the sensor position at the surface of the transmitter. The Wave system provides sensor data with respect to these global axes [2].

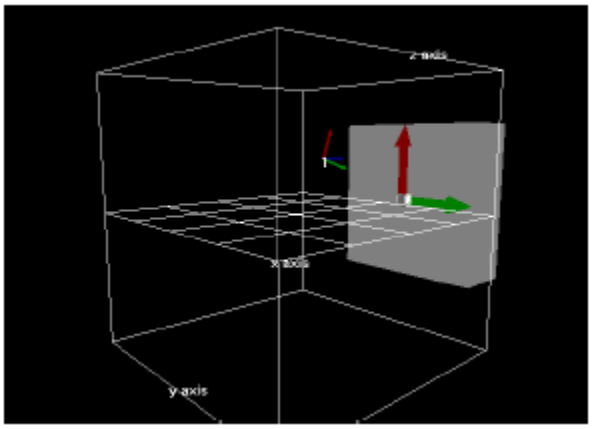

Figure 3 – Axes of the NDI Wave system, with the origin at the center of the field generator [2]

However, global position is often not useful for speech analysis, as head movements during speech production would result in movement of the articulators that is

not related to speech production. In the Marquette University Speech and Swallowing Lab, the 6-DOF sensor is attached to the bridge of a pair of glasses that is worn by the subject so that the reference sensor will experience any head movements or tremors that may take place, as seen below in Figure 4. This reference sensor allows for the creation of a new origin and new axes for the sensors [2]. The 6-DOF sensor can be used to identify these movements and how they affect each sensor by subtracting the position of the reference sensor from the absolute position of the specific sensor to obtain that sensor's head-corrected position. The NDI Wave implements this method internally.

.

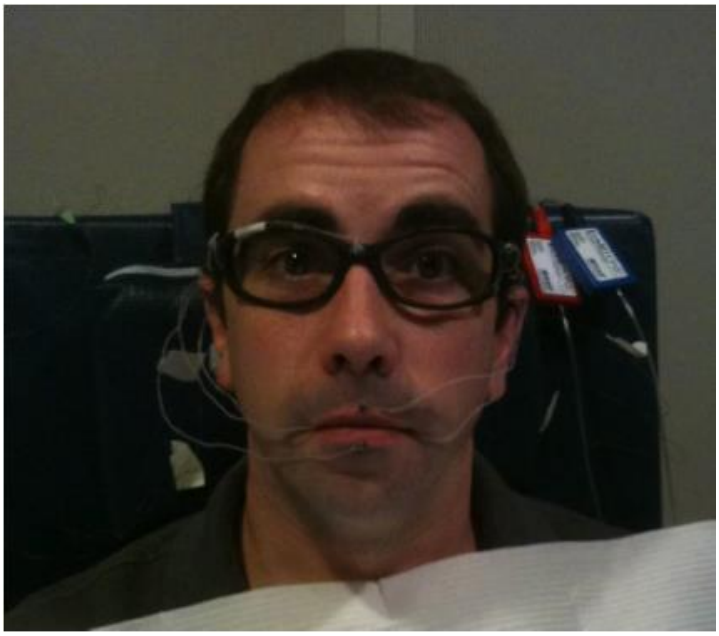

Figure 4- Subject with sensors attached to the tongue and lips and a reference sensor on the bridge of the glasses [2]

While head-correcting the data accounts for head movement, it is not optimal for representing speech articulation. The axes defined by the reference sensor are not well-defined for the end user and so attempting to identify the direction of articulator movement can be difficult. In addition, the distance between the bridge of the nose and

the articulators varies for each subject. It is thus desirable to convert the head-corrected data to a spatially normalized coordinate space that makes allowances for the differences in facial features of the subjects. This transform is known as biteplate correction, named thus because during data collection, a plate is placed between the subject's jaws for the subject to bite [2].

Biteplate correction involves the selection of a new origin and axes for the data and the implementation of a method to translate data from the previous coordinate space to the biteplate-corrected space. In the Marquette Speech and Swallowing Lab, the reference frame is selected so that the origin is at the intersection of the maxillary occlusal plane and the midsagittal plane, anterior to the central maxillary incisors. The x-axis is in the anterior direction along the midsagittal plane, while the y-axis points superior and the z-axis points to the right of the subject. The x-y plane thus becomes the midsagittal plane, and the x-z plane becomes the maxillary occlusal plane. [2] The biteplate below in Figure 5 is used to define the new origin and axes.

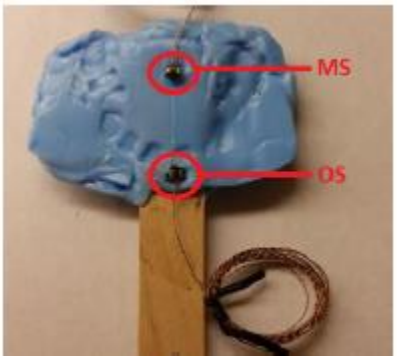

Figure 5 - Biteplate with the MS and OS sensors labeled [2]

For the biteplate correction done in the Marquette Speech and Swallowing Lab, two sensors are placed along the midsagittal line of the biteplate as shown above in Figure

5. The 6-DOF reference sensor is placed between the subject's eyes utilizing the same device as the head-correction method. The OS sensor, which defines the new origin for the biteplate-corrected coordinate space, is located on the anterior side of the central maxillary incisors when the biteplate is placed in the mouth. The line from the MS sensor to the OS sensor forms the positive x-axis, while the perpendicular component to the line to the OS sensor from the reference sensor defines the y-axis. The cross-product of these vectors is taken to form the z-axis [2].

3. EGG SYSTEM OVERVIEW

3.1 EGG Summary

The electroglottogaph system was developed to monitor the level of abduction and adduction of the vocal folds that takes place during voiced speech. Variations in vocal fold contact area (VFCA) are measured and can be used to estimate the degree of abduction, although this estimate becomes less accurate as the degree of abduction increases. VFCA measurements differ as the vocal folds vibrate because vocal fold abduction generally causes a shorter period of vocal fold contact, as well as a smaller area of contact [19].

3.2 EGG Operating Principles

The underlying principle beneath EGG operation is transverse electrical conductance (TEC). When the vocal fold contact area changes, a small change in impedance occurs. By passing a small AC current though the neck in the area of the larynx, this change in impedance can be measured and used to indicate higher or lower degrees of abduction. This current is applied through two electrodes, which are placed on the neck approximately at the level of the larynx. However, the change in conductance is often only on the order of 1% of the total conductance. The measured conductance variance additionally depends on the subject's anatomical structures surrounding the glottis, such as the location of the glottis, the degree of muscular, glandular, and fatty tissue surrounding the larynx, and thyroid cartilage structure. The electrodes may also play a role in this conductance change – if they are not placed correctly, they will not measure the correct impedance difference. In addition, if the electrodes are pressed

deeply into the neck in an area containing large amounts of subcutaneous fatty tissue, the measurement accuracy will decrease [19]. Figure 6 below illustrates the proper positioning of the electrodes on a subject's neck and how the transverse electrical conductance data is obtained.

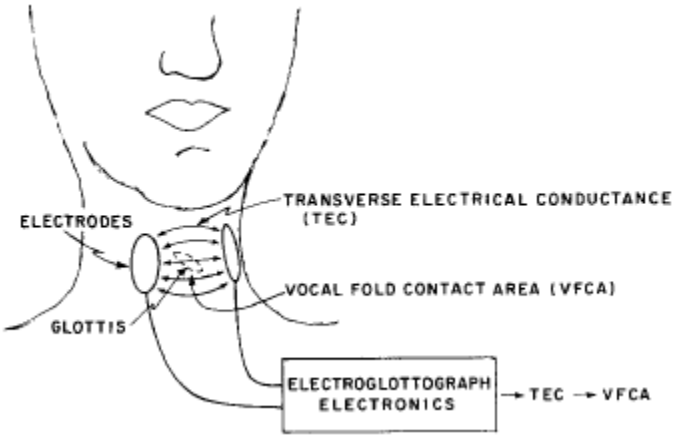

Figure 6 - Diagram of EGG positioning and use to obtain VFCA measurements [19]

Marquette University Speech and Swallowing Lab utilizes an elastic band to ensure that the electrodes fit snugly against each subject's neck with minimal discomfort and with no adhesive to add additional impedance to the system.

3.3 EGG Data Post Processing

Due to the EGG's low cost of operation, ease of use, and non-invasiveness, it has been used as a research tool for over forty years to characterize the relationship between the vocal fold vibratory events and EGG Wave aspects. This relationship, seen below in Figure 7 [20], is based on data gathered from experiments utilizing methods such as laryngeal stroboscopy, photoglottography, and inverse filtering. These model's features

were not derived from a compilation of statistical data and were instead inferred from observations and reports containing the experimental results [20].

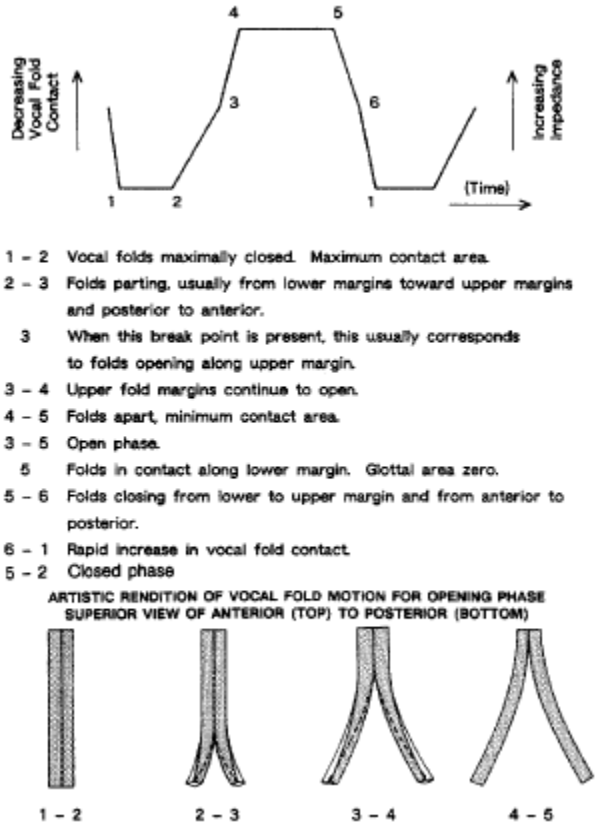

Figure 7 - Ideal EGG Waveform segment with the accompanying vocal fold events labeled [20]

A mathematical model was created by Childers, Hicks, Moore, and Alaska to characterize the EGG Waveform as a function of time, as seen below in Equation 3.3.1: [4]

$$EGG(t) = k / \left[A(t) + C \right]. \tag{3.3.1}$$

where t refers to time, k refers to a scaling constant, A(t) refers to the vocal fold contact area, and C is a constant that is proportional to the shunt impedance at A(t) = 0 [20].

The collected TEC Waveform is a composite of a frequency component that is lower than the fundamental frequency of the subject's speech and of frequency components that are harmonics of the vocal fold vibratory period, which are present at the fundamental frequency and higher frequencies. The low frequency component can be confused with low frequency noise and is thus often difficult to separate for analysis. However, if it can be separated, it contains information about average vocal fold abduction and is useful as a reference when observing abduction throughout the trial. The time constant for vocal fold abduction or adduction is similar to that of other events such as the pulsing of the carotid artery, which results in the intermingling of the low frequency component with noise [19].

An example of EGG analysis using the low frequency component can be seen below in Figure 8, which compares the low frequency component of the EGG signal with the air flow through the glottis as a male adult subject spoke the phrase, "The hut." The EGG signal is inverted so that increased contact is indicated by a spike in the negative direction. This is a standard representation, as an increase in air flow is associated with a decrease in contact. Even though the speech was voiced during the entire phrase, as evidenced by the constant flow of air through the glottis, the EGG signal indicates that when the "h" was pronounced, there was no contact by the vocal folds – the downward spike that is associated with an increase in contact is not present during those cycles. Since there is variation in the glottal air flow during this time, this indicates that there was vocal fold movement. This further indicates that there was no vocal fold contact while the 'h" was pronounced; movement of the vocal folds would have resulted in

variation in the amount of contact if a significant area of the vocal folds were already in contact [19].

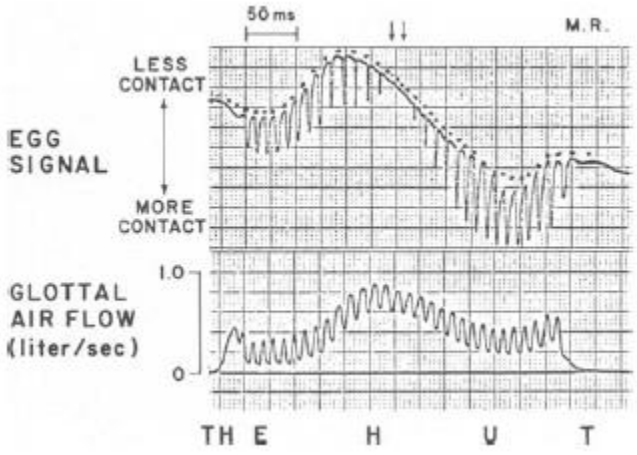

Figure 8 - Glottal air flow and low frequency component of the EGG signal during an adult male subject's pronunciation of the phrase, "the hut" [19]

However, the low frequency component must be obtained by modified EGGs that are configured to increase the high-pass time constants in the feedback path of the control circuit that adjusts the amount of current passed through the neck.

Figure 9 below shows the same phrase with the upper frequency components of the EGG represented in the inverted VFCA waveform. As seen, as the vocal folds are abducted, the average air flow generally increases. During the abduction process right before the “h”, the oscillations of the vocal fold contact area, representing closed-phase periods, decrease in width until there is only a single narrow pulse. At the pronunciations of the “h”, there is no vocal fold contact. After the “h”, adduction occurs and oscillations of the vocal fold contact area increase in width once more [19].

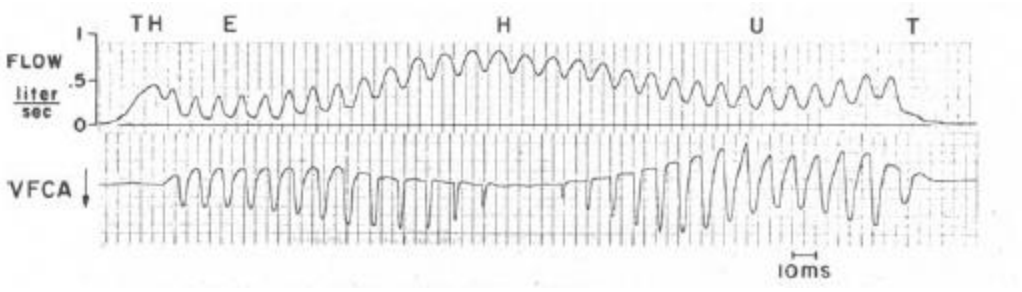

Figure 9 - Glottal air flow and the high frequency components of the EGG signal during an adult male's pronunciation of the phrase, "the hut" [19]

Different vocal fold vibratory or glottal area events have been assumed to be related to specific segments of either the EGG or the differential EGG (DEGG) signal, which are shown below in Figure 10. These include the moments of the opening of the glottis and of the positive peak of the DEGG, as well as the moments of the closing of the glottis and of the negative peak of the DEGG. In addition, the moment of the maximum glottal area and the moment of the maximum positive peak of the normalized EGG waveform are also hypothesized to be related.

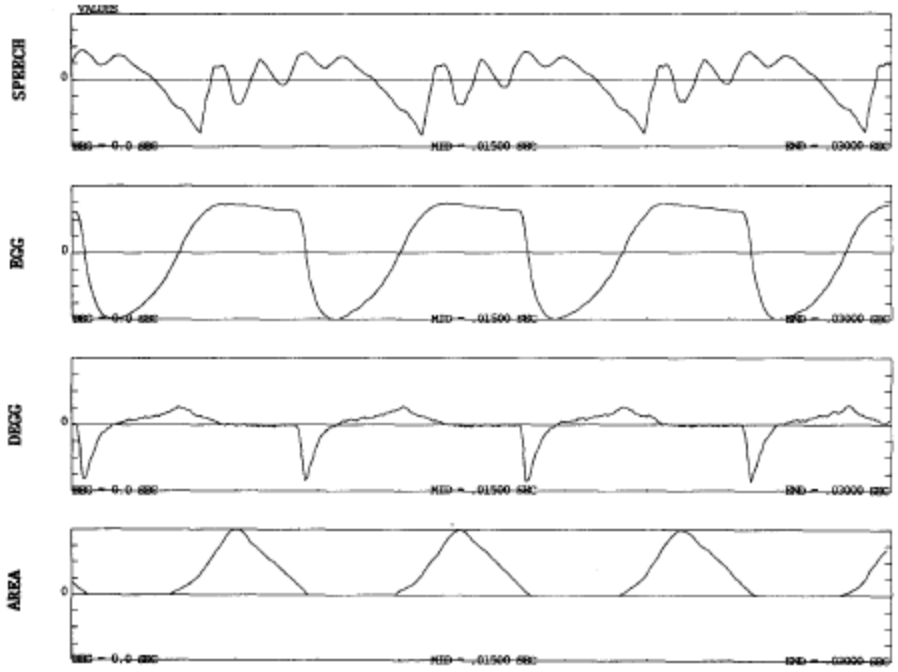

Figure 10 - Data Waveforms from a male subject with F0 at approximately 120Hz. [20]

There are two additional parameters that can be used for analysis, with each being found from glottal area and compared with the measured value from the EGG Waveform. The first is the open quotient, which can be calculated using Equation 3.3.2 below:

$$OQ = \frac{duration\ of\ \ glottal\ \ phase}{duration\ of\ \ glottal\ cycle}. \tag{3.3.2}$$

The second parameter is relative average perturbation (RAP), which can be measured from the glottal area and EGG Waveforms [20]. RAP can be defined as the equation below:

$$RAP = \left[\frac{1}{N}\sum_{i=1}^{N} P(i)\right]^{-1} \frac{1}{N-2}\sum_{i-2}^{N-1}\left|\frac{P(i-1)+P(i)+P(i+1)}{3} - P(i)\right|. \tag{3.3.3}$$

4. INITIAL DETERMINATION OF INTERFERENCE

4.1 Methodology

Eleven trials were conducted to investigate the degree of interference between the EGG and EMA systems. In each, a subject held a biteplate in a given position in the field. For each given position, the EGG sensors were alternately not present, present with the EGG system turned off, present with the system turned on, and present with the system turned on and the subject vocalizing.

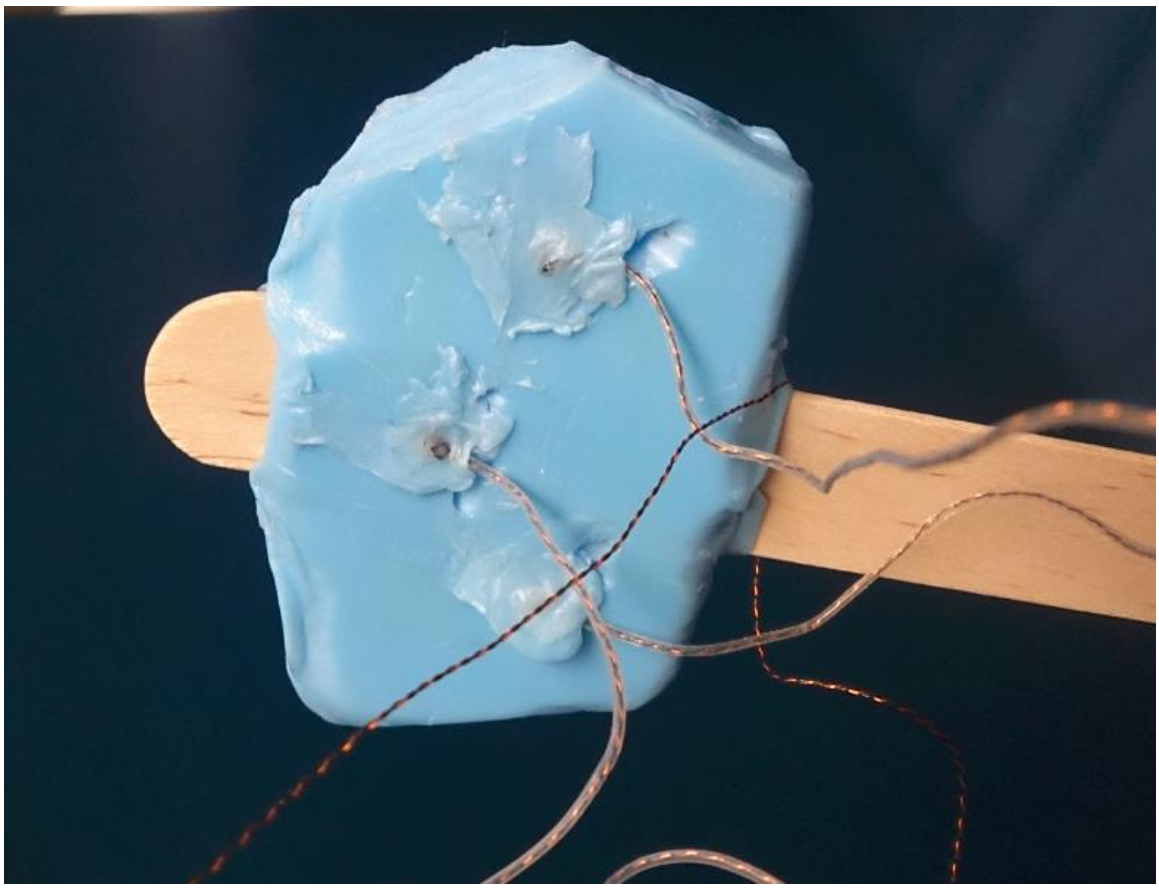

Figure 11 - Biteplate used for stationary trials, with the lowest sensor being sensor 1, the middle sensor being sensor 2, and the highest sensor as sensor 3

One objective was to identify the optimal field location of the biteplate and EGG sensor combination. The NDI Wave has been shown to have higher accuracy when the

EMA sensors are located in the center of the field [11]; however, it was hypothesized that interference from the EGG sensors might be lesser if the EGG sensors were located at the edge or outside of the electromagnetic field. Three likely positions for the systems were determined: EMA sensors and EGG electrodes placed in the center of the field, EMA sensors and EGG electrodes set at the edge of the field, and EGG electrodes outside of the field with the EMA sensors at the edge of the field. For each trial, the bite plate was initially oriented with the sensors on the same horizontal plane and located in front of the subject's lower jaw, positioned so that sensor 2 was closest to the jaw.

Two baseline data sets were first collected: one in which the subject was in the center of the field and the other in which the subject was located at the edge of the field. Baseline data sets refer to data sets in which only the EMA is present, without the EGG or any other source of interference. No baseline was collected for when the EGG would be outside the field – since the EMA sensors would be located at the edge of the field, that baseline was deemed to be sufficient. The EMA baseline data from the edge of the field was used for comparison for the trials in which the EGG sensors would be outside of the field.

The EGG electrodes were then strapped to the subject's throat at the approximate location of the vocal folds. A fourth EMA sensor was attached to the electrodes so that it would be possible to see whether the EGG electrodes were in the field. The EGG system was first turned off when attached to the subject, and data sets were collected from each of the locations in the field. While the EGG system would not be turned off during a study, this helped to establish whether interference would result solely from the presence

of the EGG electrodes in the electromagnetic field or was a combination of the presence of the sensors and use of the system.

The EGG system was then turned on while the subject remained quiet, and data sets were then collected from each of the field positions. Data collection from each of the locations was then repeated with the EGG system turned on and the speaker vocalizing the vowel “ah” for as long as was possible.

Table 1 - Different trials run in order to ensure accurate representations of each location in electromagnetic field and state of EGG

Center			
EGG not worn (base)	EGG turned off	EGG turned on	EGG on, vocalized

Edge			
EGG not worn (base)	EGG turned off	EGG turned on	EGG on, vocalized

Outside		
EGG turned off	EGG turned on	EGG on, vocalized

4.2 Analysis Methods

Two assessment criteria were determined to identify whether there was the presence of metal produced a significant impact on the EMA data for inter-sensor distance. The first was the determination of the resulting bias on the inter-sensor distance measurement. The bias can be defined as the difference between the baseline inter-sensor Euclidian distance and the inter-sensor Euclidian distance when a source of interference was present. The second criterion is the standard deviation of the signal. The presence of metal could cause additional noise to be present in the signal, and so the standard deviations of the baseline signal and of the signal with a source of interference present

were noted. The bias and standard deviation can then be added to identify the approximate maximum error of the signal. The maximum error should be below $\pm$0.5 mm, which is the accepted NDI Wave error in sensor position, because any interference should be such that the NDI Wave error specifications are maintained. Since the sensors were rigidly attached, the distance between each sensor pair should be fixed with a bias of 0 mm, and have a standard deviation of 0 mm. A nonzero standard deviation and bias in the presence of metal indicate that there has been interference as a result of the metal.

The inter-sensor angle bias and standard deviations were found to better characterize the accuracy of the orientation data gathered with metal in the field. The rigid attachment of the sensors results in a constant angular orientation, with a standard deviation of 0° and a bias of 0°. A nonzero bias and standard deviation indicate that interference has occurred. However, there are no formal system specifications for orientation accuracy, so these results are presented as a way to obtain a better understanding for how orientation data is affected by the presence of metal.

4.3 Results

The inter-sensor distance trials were conducted in the center of the field, the edge of the field, and with the EGG sensors outside the field and the EMA sensors at the edge of the field. Since the results from each sensor pair contained similar trends, only the data from sensors 1 and 2 is presented below. The data from the other sensors is shown in Appendix A.

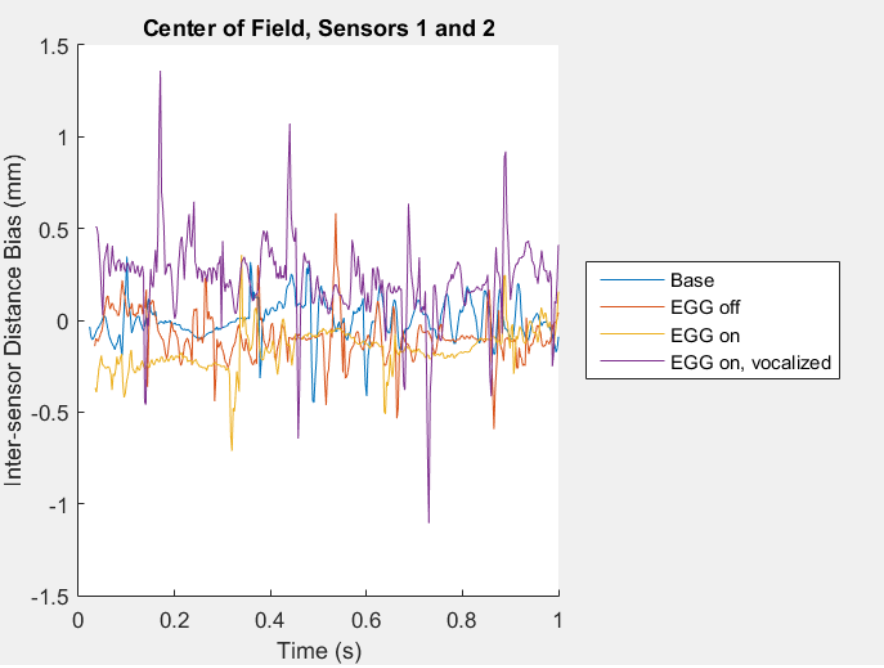

Figure 12 – Inter-sensor distance biases for sensors 1 and 2 for four interference conditions when sensors are stationary and in center of field

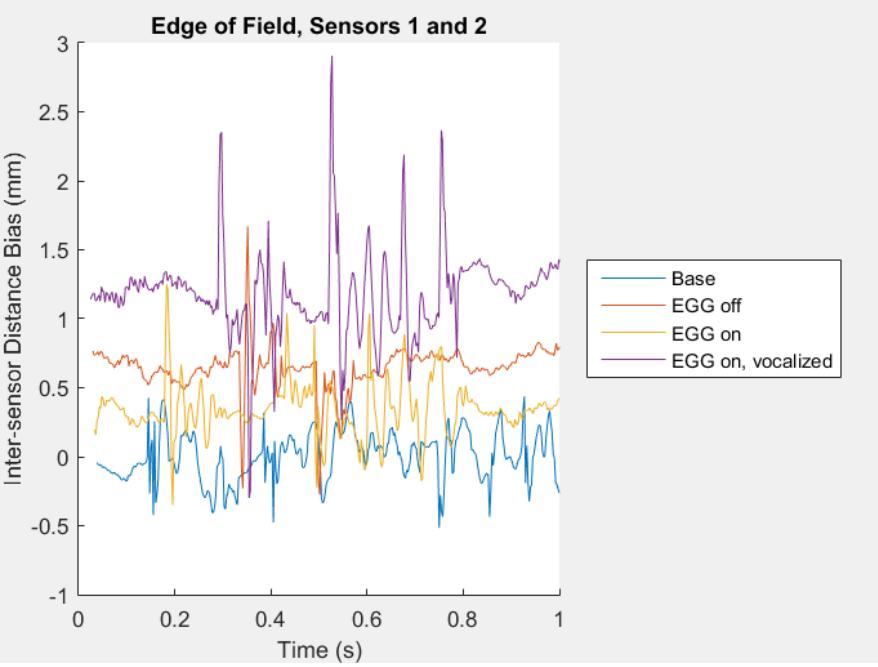

Figure 13 – Inter-sensor distance biases for sensors 1 and 2 for four interference conditions when sensors are stationary and are at edge of field

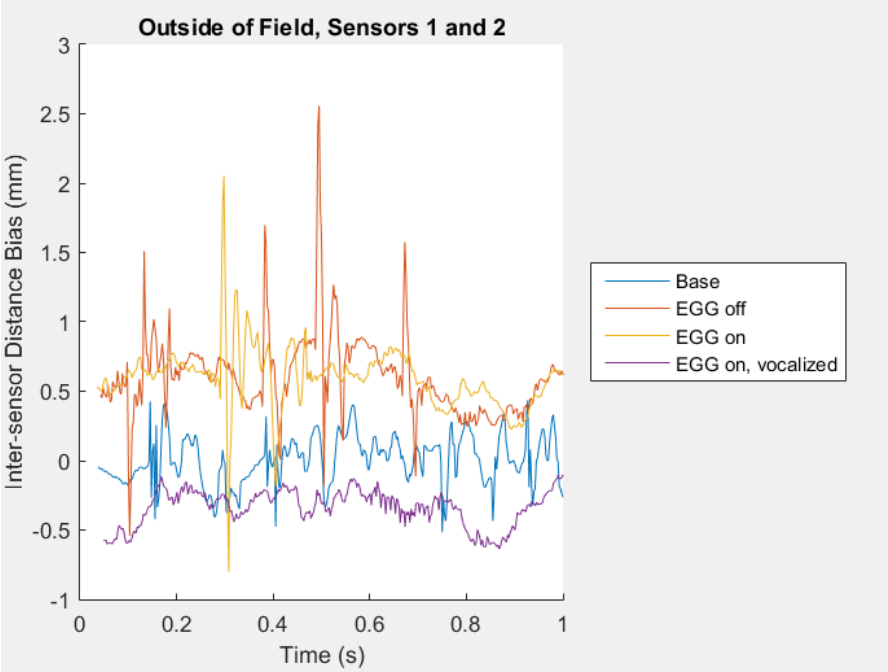

Figure 14 – Inter-sensor distance biases sensors 1 and 2 for four interference conditions when sensors are stationary and EGG sensors are outside of the field

The biases for each trial were calculated and can be seen below.

Table 2 - Comparison of average baseline inter-sensor distance with average inter-sensor distance of each interference trial at center of field

Trial condition (center)	Inter-sensor distance (mm)	Bias (mm)	% difference
Baseline	19.123	------	------
EGG off	19.036	-0.087	-0.452
EGG on, unvocalized	18.962	-0.161	-0.841
EGG vocalized	19.346	0.224	1.169

Table 3 - Comparison of average baseline inter-sensor distance with average inter-sensor distance of each interference trial at edge of field

Trial condition (edge)	Inter-sensor distance (mm)	Bias (mm)	% difference
Baseline	18.705	------	------
EGG off	19.349	0.645	3.448
EGG on, unvocalized	19.048	0.344	1.837
EGG vocalized	19.888	1.184	6.330

Table 4 - Comparison of average baseline inter-sensor angle with average inter-sensor angle of each interference trial when EGG sensors were outside of field

Trial condition (outside)	Inter-sensor distance (mm)	Bias (mm)	% difference
Baseline	18.705	-----	------
EGG off	19.306	0.601	3.214
EGG on, unvocalized	19.297	0.593	3.169
EGG vocalized	18.371	-0.334	-1.783

The maximum error of the measurements for each trial were calculated by adding the bias and the standard deviation.

Table 5 - Maximum error when systems are stationary and present in center of field

	Bias (mm)	Standard deviation (mm)	Maximum error (mm)
Baseline	0	0.106	0.106
EGG off	-0.087	0.125	-0.212
EGG on, unvocalized	-0.161	0.113	-0.274
EGG on, vocalized	0.224	0.218	0.442

Table 6 - Maximum error when systems are stationary and present at edge of field

	Bias (mm)	Standard deviation (mm)	Maximum error (mm)
Baseline	0	0.179	0.179
EGG off	0.645	0.160	0.805
EGG on, unvocalized	0.344	0.193	0.537
EGG on, vocalized	1.184	0.311	1.495

Table 7 - Maximum error when systems are stationary, the EGG sensors are outside of the field, and the EMA sensors are at the edge of the field

	Bias (mm)	Standard deviation (mm)	Maximum error (mm)
Baseline	0	0.1786	0.179
EGG off	0.601	0.2989	0.900
EGG on, unvocalized	0.593	0.2251	0.818
EGG on, vocalized	-0.334	0.1314	-0.465

The orientation data was also analyzed to calculate the inter-sensor angle biases and standard deviations.

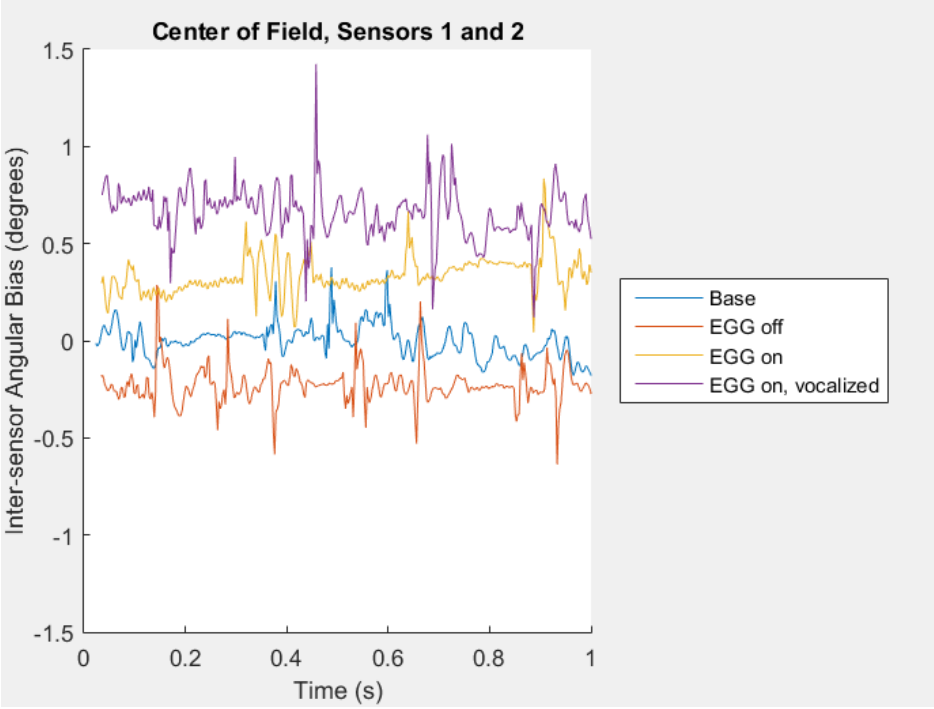

Figure 15 – Inter-sensor angular biases when the systems were in the center of the field

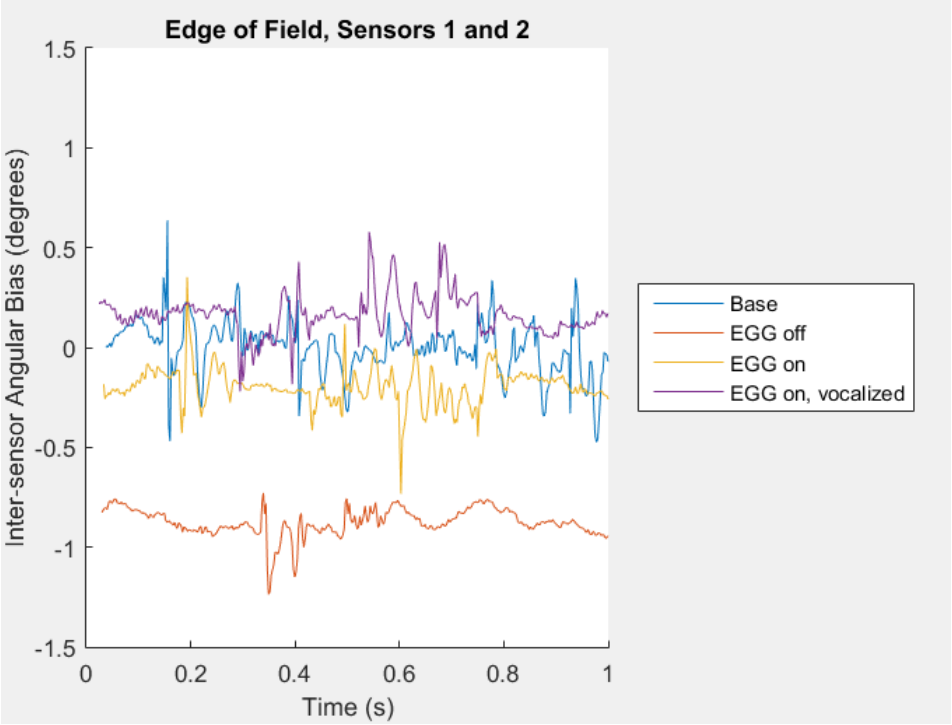

Figure 16 – Inter-sensor angular biases for sensors 1 and 2 in the stationary trials when the systems were at the edge of the field

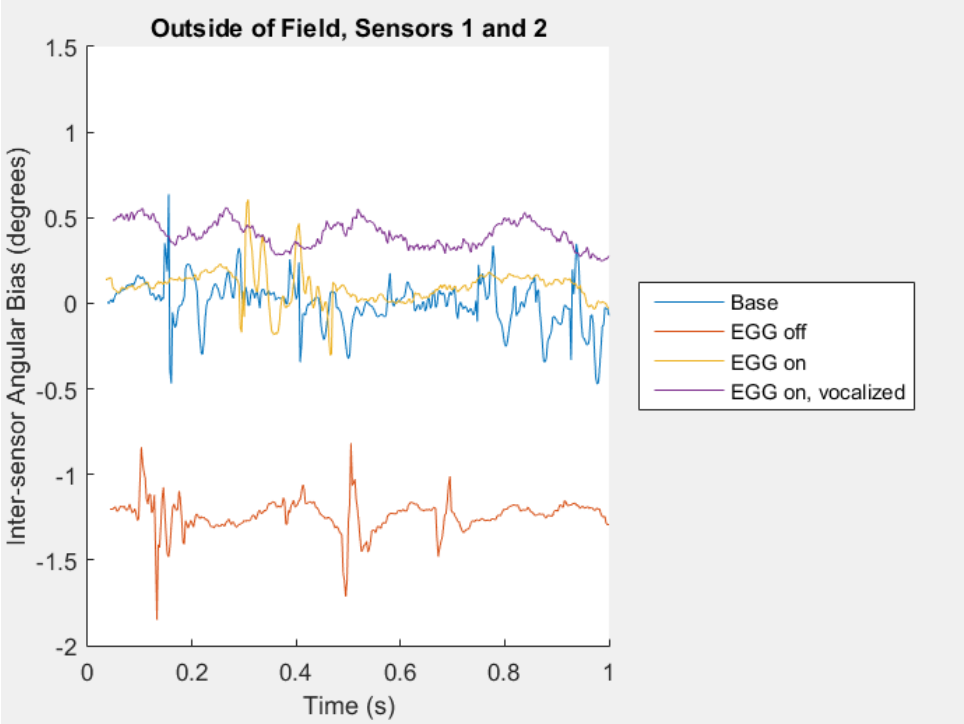

Figure 17 – Inter-sensor angular biases for sensors 1 and 2 in the stationary trials when the EGG sensors were outside of the field

Table 8 - Comparison of average baseline inter-sensor angle with average inter-sensor angle of each interference trial at center of field

Trial condition (center)	Inter-sensor angle (°)	Bias (°)	% difference
Baseline	22.822	------	------
EGG off	22.592	-0.229	-1.005
EGG on, unvocalized	23.159	0.338	1.480
EGG vocalized	23.483	0.661	2.898

Table 9 - Comparison of average baseline inter-sensor angle with average inter-sensor angle of each interference trial at edge of field

Trial condition (edge)	Inter-sensor angle (°)	Bias (°)	% difference
Baseline	22.822	------	------
EGG off	21.947	-0.874	-3.831
EGG on, unvocalized	22.626	-0.196	-0.859
EGG vocalized	22.984	0.162	0.710

Table 10 - Comparison of average baseline inter-sensor angle with average inter-sensor angle of each interference trial when EGG sensors were outside of field

Trial condition (outside)	Inter-sensor angle (°)	Bias (°)	% difference
Baseline	22.822	-----	------
EGG off	21.582	-1.239	-5.431
EGG on, unvocalized	22.918	0.096	0.419
EGG vocalized	23.222	0.400	1.752

The maximum error for each trial was then calculated by adding the bias and standard deviation.

Table 11 - Maximum error when systems are stationary and present in center of field

	Bias (°)	Standard deviation (°)	Maximum error (°)
Baseline	0	0.081	0.081
EGG off	-0.229	0.092	-0.137
EGG on, unvocalized	0.338	0.097	0.435
EGG on, vocalized	0.661	0.127	0.788

Table 12 - Maximum error when systems are stationary and present at edge of field

	Bias (°)	Standard deviation (°)	Maximum error (°)
Baseline	0	0.136	0.136
EGG off	-0.874	0.069	-0.943
EGG on, unvocalized	-0.196	0.091	-0.287
EGG on, vocalized	0.162	0.101	0.263

Table 13 - Maximum error when systems are stationary, the EGG sensors are outside of the field, and the EMA sensors are at the edge of the field

	Bias (°)	Standard deviation (°)	Maximum error (°)
Baseline	0	0.136	0.136
EGG off	-1.239	0.095	-1.334
EGG on, unvocalized	0.096	0.103	0.199
EGG on, vocalized	0.400	0.078	0.478

4.4 Discussion

The ideal location for the EGG and EMA sensors would be the location in which there was the lowest sensor error. Examining Table 5, Table 6, and Table 7 shows that the lowest maximum errors occurred when the EGG and EMA sensors were located in the center of the field. Table 5 shows that the in the center of the field, the highest error was 0.442 mm. While high, it is still/ beneath the NDI specification of 0.5 mm. In contrast, when both EGG and EMA sensors were located at the edge of the field, the maximum error for the EGG and subject vocalization was over 0.5 mm for every trial except the baseline. The maximum errors of the system were slightly lower when the EGG was out of the field while the EMA was at the edge of the field, but two of the four trials had an error larger than 0.5 mm.

By comparing Table 11, Table 12, and Table 13, it can be seen that the inter-sensor angle did not quite follow this trend. The average maximum error for the trial in the center of the field was lower than that of the trial at the edge of the field and the trial with the EGG outside of the field.

Due to the overall lower inter-sensor distance and angle errors present at the center of the field, the center of the field will be used as the location for the EGG and EMA systems for both further analysis and trials. This was additionally desirable because of difficulties ensuring that the EMA sensors remained within the field when positioned at the edge of the field and having the subject vocalize. Difficulties also arose with preventing the EGG sensors from entering the field during the trials in which the EGG sensors were supposed to be outside of the field.

Table 5 shows that when the EGG was present, there was a higher error than in the baseline data. The highest error value occurred when the EGG was on and the subject was vocalizing. However, the error of 0.442mm is still within the NDI Wave system specifications.

The interference present in the different trials was additionally examined through the orientation information for each trial. Since the bite plate was held relatively stable for each trial, the maximum error of the inter-sensor angle values was expected to be small. The results, seen in Table 11, show that the highest error present was below 0.8°, which is relatively small. However, there was a noticeable increase in error with the addition of the EGG and the vocalization of the subject.

The trial that involved the subject vocalizing with the EGG present showed the most amount of error. The vocalization of the subject, though, should not have a significant impact on the error in theory. The current passing through the vocal folds is minimal, and is being applied regardless of whether the subject is vocalizing. Therefore, the EMA sensors should be affected by the EGG sensors in the same way for subject vocalization and subject silence. One hypothesis was that during the vocalization trial, the subject's hand occasionally appeared to tremble as the sound was held. The shaking of the biteplate may have caused incorrect sensor readings, which in turn would have contributed to the higher error rate.

In the presence of the EGG, the EMA sensors performed within the NDI error specifications with regards to inter-sensor distance and had small errors in terms of inter-sensor angle.

5. DETERMINATION OF EFFECTS OF VELOCITY ON ACCURACY

5.1 Purpose

The previous trials used to investigate the interference between the EGG and EMA systems were conducted in static conditions. Ignoring slight variability due to minute movements of the hand holding the bite plate and the throat, the systems were approximately at rest. However, for clinical applications, the systems would be used while the subject was talking, resulting in a nonzero velocity for the EMA sensors. It was thus necessary to investigate the effects of velocity upon the EMA sensors, both when the EGG was present and when it was absent.

5.2 Construction of Model

The electromagnetic field used by the EMA system acted as a design constraint for the model that would ensure constant movement of the sensors. No metal could be used in the construction of the rotation model without the risk of additional interference. Therefore, the final design was constructed out of plastic Lego pieces. A wooden platform was constructed to hold a group of sensors in a constant orientation. Two shafts were then attached to this platform at either end. These shafts interacted with a longer perpendicular shaft through gears. When the longer shaft was rotated from a distance away, the gears rotate, forcing the shorter shafts to rotate and to move the platform in a circle. Since the lab's NDI system has a field that is a 300mm cube, the longer shaft was constructed so that when the platform was rotated, the attached motor would still be outside of the field. A water-based lubrication was applied to the ends of the shorter shafts before operation in order to ensure a smoother rotation.

The movement of the non-ferrous rotation model mimicked the movement of the articulators, with the positive y-direction representing the anterior-most of the sensors. To accurately reflect the clinical placement of the EGG with respect to the EMA sensors, the EGG sensors were positioned around a tube placed on the posterior side of the trajectory of the sensor platform.

The motor was selected so that target mean articulator speeds could be achieved. In 2004, a study by Tasko and Westbury showed that when speakers spoke the words "doors back to the places," the maximum articulator speed was approximately 120mm/s [21]. This was later supported by Bauer et. al in 2010, who found that mean speeds of the labial movements, tongue tip movements, and tongue body movements are approximately 118mm/s, 125mm/s, and 84mm/s respectively [22]. Based on this, a target sensor velocity of 125mm/s was selected.

The construction of the non-ferrous rotation model allowed for radii of rotation ranging between approximately 5mm to 60mm. As the length of the oral cavity is approximately 50mm to 60mm, it was decided that the radius of model rotation would be approximately 30mm.

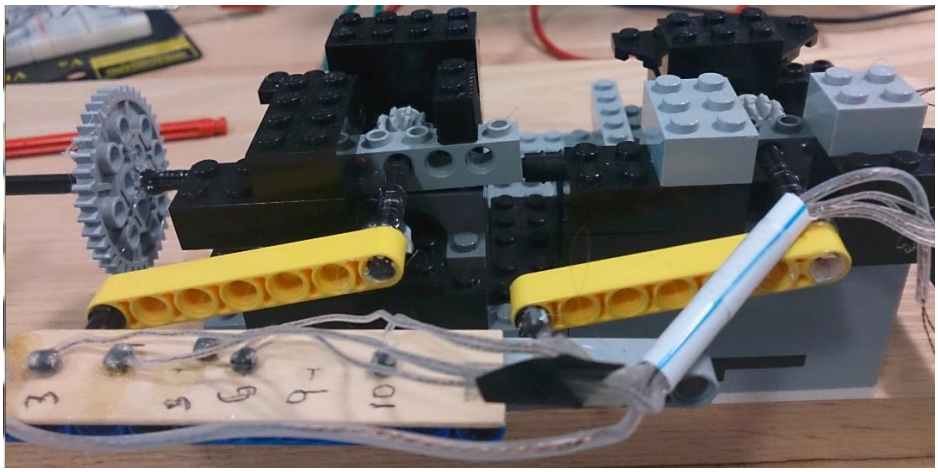

(a)

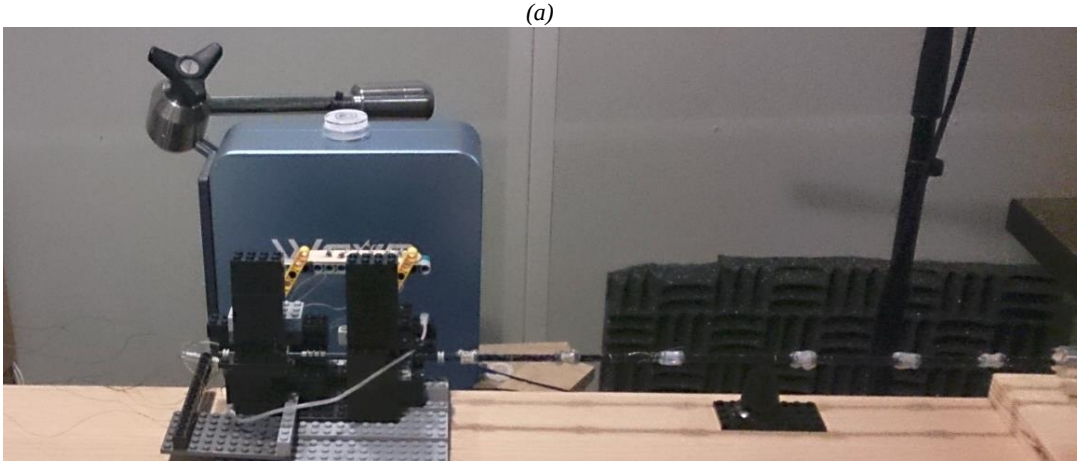

(b)

Figure 18 – The final Lego model and experimental setup.

Figure 18(a) displays the rotating platform with the majority of the sensors attached. Figure 18(b) displays the setup of the model with respect to the field generator. The long shaft extending to the right is connected to the motor, which rotates the long shaft and thus the platform.

The diagram below in Figure 19 shows the approximate motion of the non-ferrous rotation model traced by the dotted circles.

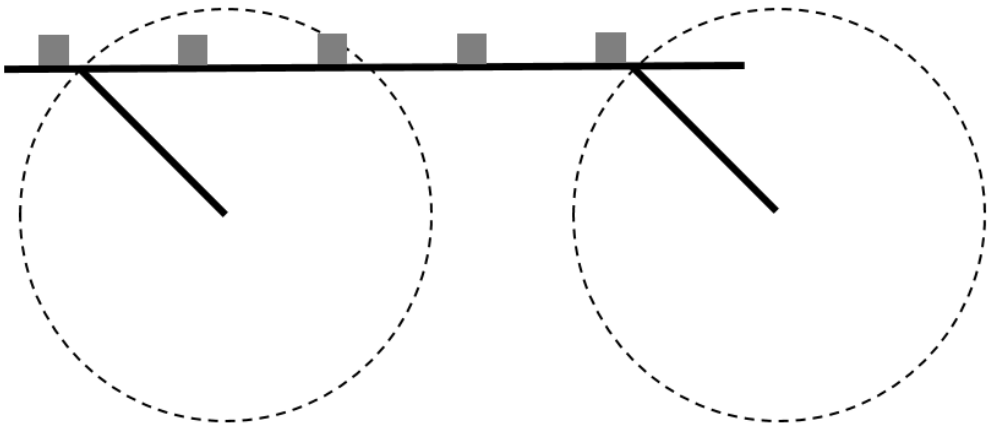

Figure 19- Path of the sensors on platform of model

The dotted circles underscore the identical diameters of rotation that each end of the platform travels. Each sensor travels an identical, parallel path at approximately 125mm/s; therefore, each sensor experiences identical translational velocities with no change in orientation.

5.3 Baseline Data Collection

5.3.1 Methodology

Initial data was first gathered to ensure that the model could achieve the desired speed and rotation without introducing significant variance at different speeds. Since the motor selected was a 12 V DC motor, data was collected for ten second intervals at 0.5 V steps between 0 V and 12 V. The model was positioned approximately in the center of the field with six sensors attached to the platform. Figure 20 below shows the arrangement of the sensors.

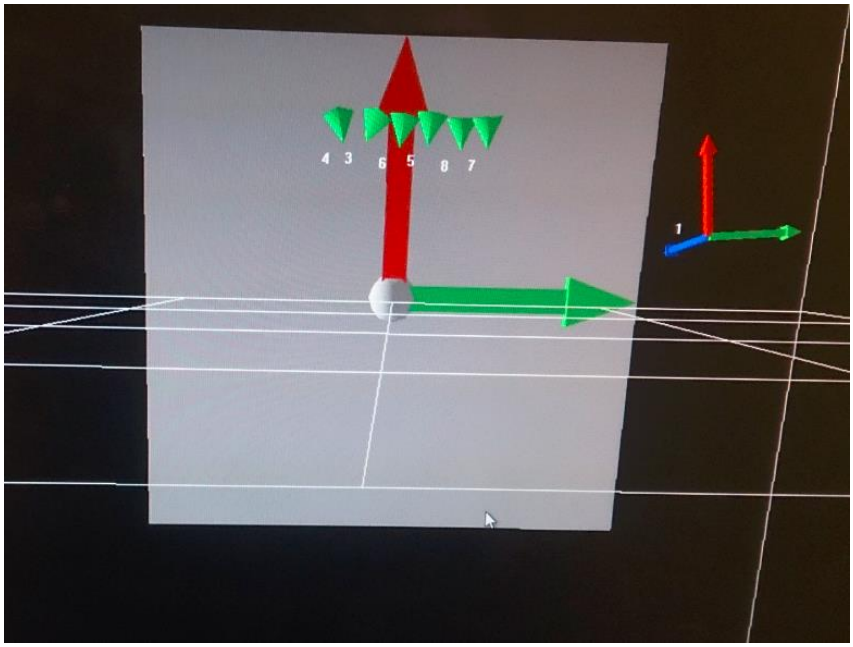

Figure 20 - Arrangement of the sensors on the non-ferrous rotation model.

The red arrow represents the x-direction while the green arrow represents the y-direction and the blue arrow gives the z-direction. The sensor labeled "1" is a stationary reference sensor positioned to give a clearer understanding of sensor orientation and to allow for non-global coordinates to be used if desired.

The resulting data sets were then analyzed with the help of Matlab. For each voltage level, the velocity of the platform was calculated by averaging the velocity of each sensor. The instantaneous sensor velocity was found using the equation below:

$$v[t] = \frac{\Delta d}{2\Delta t} \tag{5.3.1}$$

where $v[t]$ represents the velocity at time t, Δd represents the distance traveled between the sensor's positions at time [t-1] and time [t+1], and Δt represents the sampling period of the dataset.

The Euclidean distance was calculated between each adjacent pair of sensors. While non-adjacent pairs of sensors could also have been used for analysis, adjacent pairs of sensors were separated by close to a centimeter, which reflects a reasonable clinically useful distance. The average distance was then found for each sensor pair and used to zero-mean the distance values to find the bias.

In addition, the inter-sensor angle pertaining to each adjacent sensor pair was also calculated using Equations 2.4.19 and 2.4.20. The average inter-sensor angle was also found and used to zero-mean the inter-sensor angle for the sensor pair to detect angular bias.

5.3.2 Baseline Results

After analysis, it was determined that applying a supply voltage of 11.5 V to the motor resulted in the sensors moving at a translational velocity of 125.794 mm/s. Since this was the closest to the maximum average speed of 125 mm/s listed by Bauer, this supply voltage and the resulting data will be the focus of the following data analysis. Plots showing data from a select range of trials are presented in Appendix B for further review if desired.

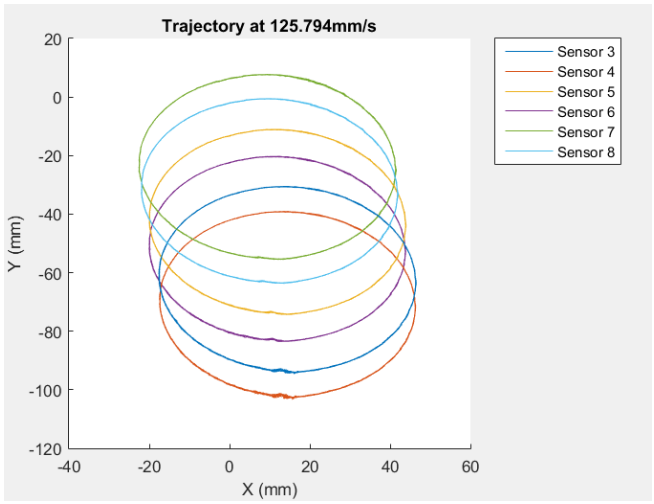

(a)

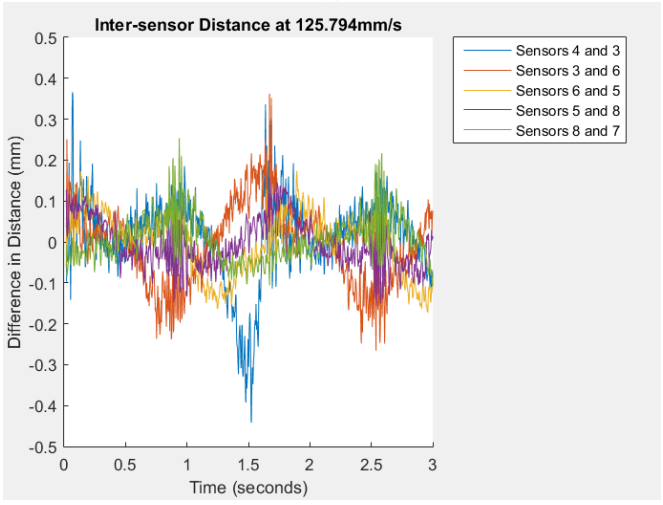

(b)

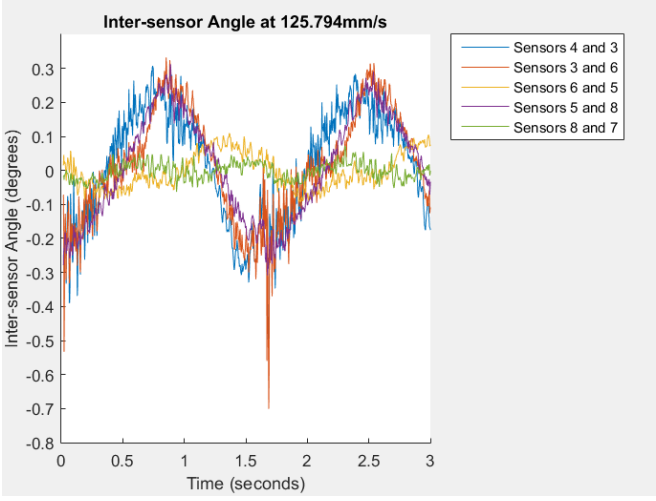

(c)

Figure 21 - Baseline results with the sensors moving at 125.794mm/s.

Figure 21(a) shows the trajectory of each sensor. It should be noted that at the point in the rotation when the minimum y-value occurred, there is a part of the trajectory that appears rougher than the rest. Figure 21 (b) shows the distance between sensor pairs after zero-meaning. Figure 21(c) shows the inter-sensor angle between sensor pairs after zero-meaning.

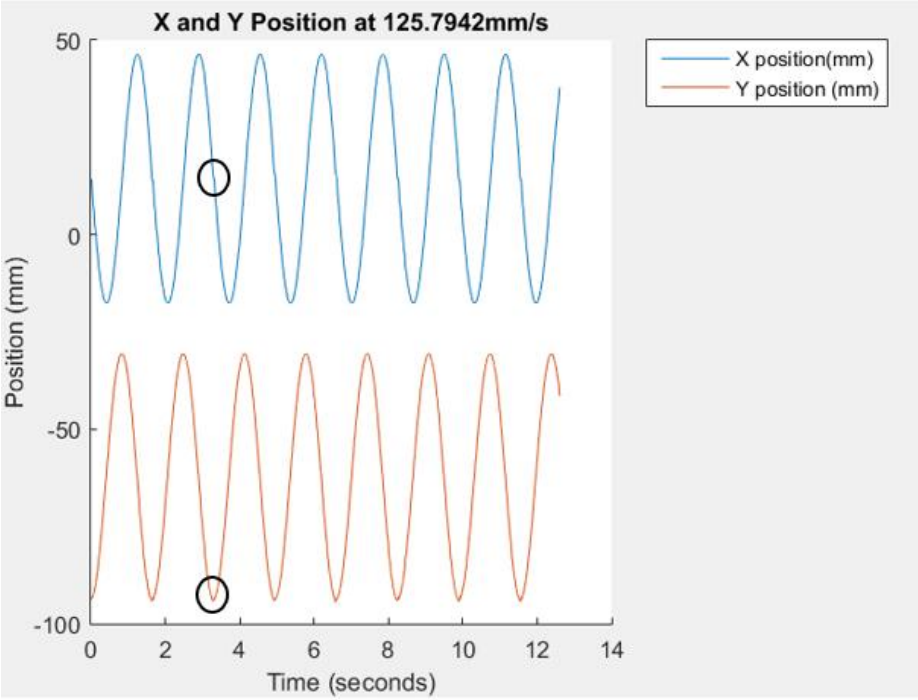

Figure 22 - Moment in which physical jerk occurs

The average inter-sensor distance and angle are recorded below, along with their respective standard deviations.

Table 14 – Stationary baseline inter-sensor distance and angle for non-ferrous rotation model

	Inter-sensor Distance (mm)	Inter-sensor Angle (°)
Average	9.223	3.300
Standard deviation	0.010	0.006

5.3.3 Baseline Results Discussion

As seen above in Figure 21, the distance bias and inter-sensor angular bias graphs show peak differences at the same time points. This is made clear by examining Figure 21(a) above. In the trajectory when the y-value is minimal, there is a part of the trajectory that does not follow the smooth oval path that occurs during the remainder of the rotation. This can be further understood by examining Figure 22 below.

In the circled regions above in Figure 22, there is a slight discrepancy that takes the form of a bump in the waveform. This was also observed during operation of the model – while the model was rotating, there was a slight jerk that occurred at the minimum y-position. As this jerk occurred more quickly than the rest of the rotation, the distance and inter-sensor angle calculated at this time differed more significantly than the mean and thus resulted in the spikes observed in Figure 21. It is hypothesized that this additional physical stress to the model may have created a small amount of movement in the model itself so that the spikes that occur at that point represent true model change rather than error in the EMA system. Regardless of this hypothesis, however, the spikes within the distance data still were within the $\pm$ 0.5 mm target value.

5.4 Analysis with Interference Sources

5.4.1 Methodology

The primary source of interference under investigation was the EGG. In order to replicate a clinical setup, the EGG sensors were attached around a piece of foam that was wrapped around a cardboard tube in order to simulate placement of the sensors on the throat.

In addition to the EGG, another source of potential interference in clinical situations is orthodontia. A retainer and palate expander were presented as standard examples of orthodontia that may be present in a subject's mouth during a clinical study. A stand was erected on the rotation model so that the dental appliances would remain approximately 1 cm above the platform at its peak rotation. Since it was determined unlikely that the subject would be wearing both a retainer and expander at the same time, the two appliances were tested separately.

Using the velocities calculated from the baseline analysis, a range of velocities between 25 mm/s and 125 mm/s were selected to represent the movement of the articulators. The corresponding supply voltages were then applied to the motor for 10 second intervals per voltage level for each trial. There was a total of five trials, corresponding to the five possible arrangements of interference sources: EGG only, EGG with retainer, EGG with expander, retainer only, and expander only. Figure 23 below shows the experimental setup:

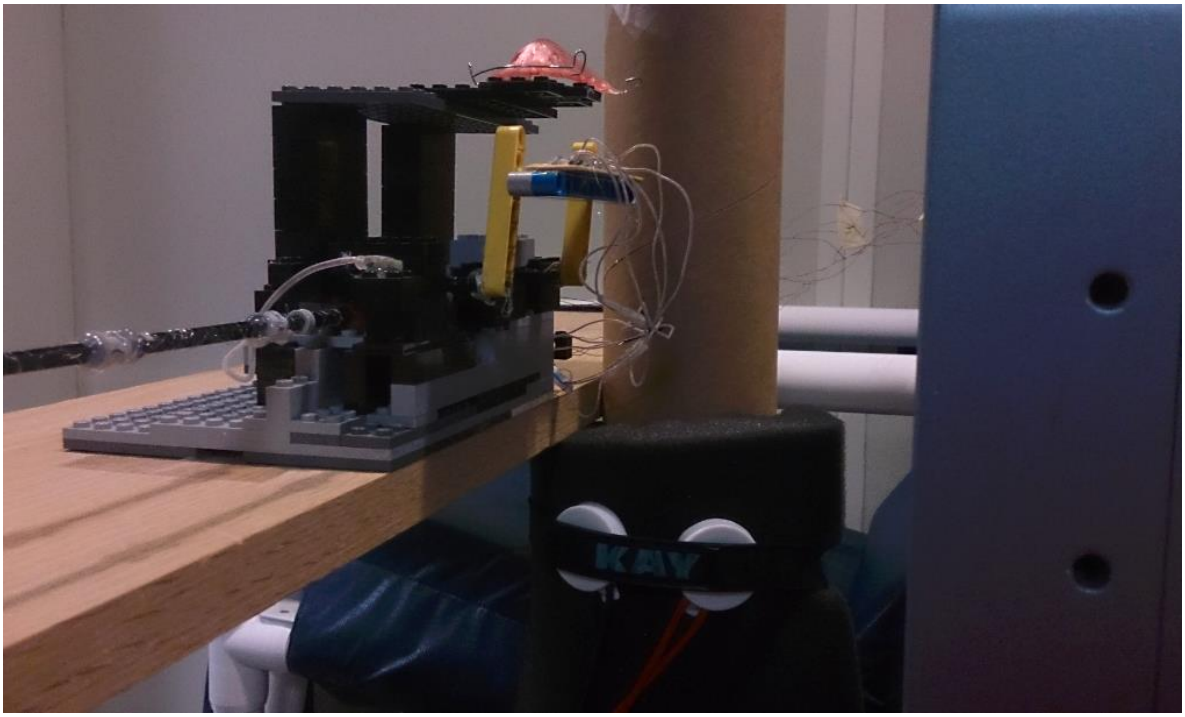

Figure 23 - Experimental setup of the non-ferrous rotation model

The retainer is located on a stand approximately 2 cm above the EMA sensors, while the EGG sensors are attached to the column below

As with the baseline data sets, the distance and inter-sensor angle between adjacent sensor pairs were found. The inter-sensor distance and angular biases were found by subtracting the average inter-sensor distance and angle from the trial distances and angles.

$$zero_{distance4to3} = \text{distance}_{4to3} - mean_{baselinedistance4to3}. \quad (5.4.1)$$

5.4.2 Results with Interference

Figure 24 below shows the difference between the average baseline distance between sensors 6 and 5 and the distance measured in trials with different sources of interference present. Results for all sensor pairs showed similar characteristics so for

simplicity, only data from sensors 6 and 5 is presented in the figures below; plots containing data from the other sensors are presented in Appendix B.

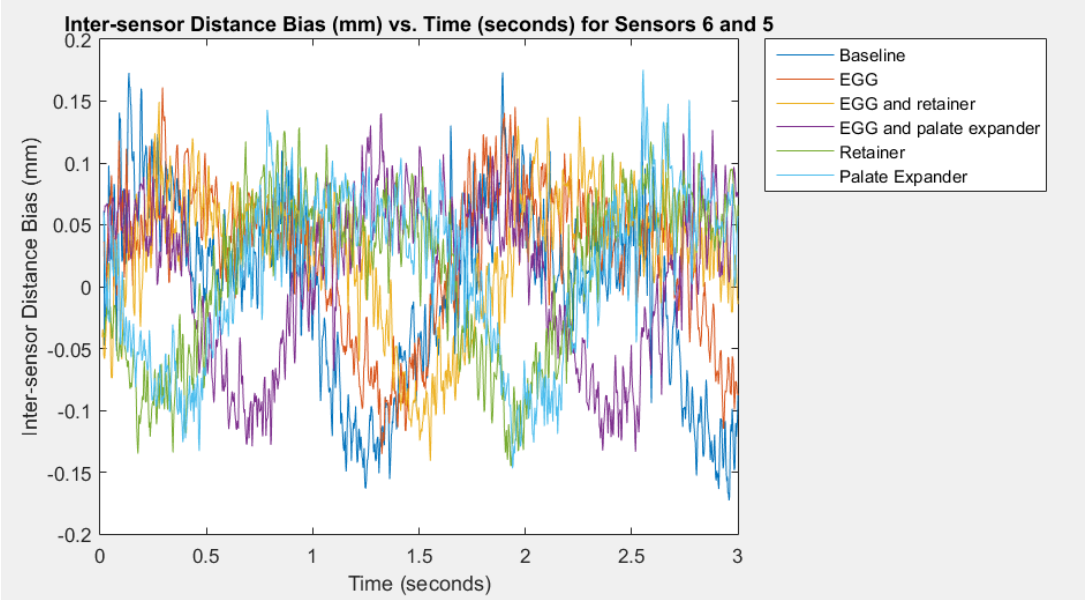

Figure 24 – Inter-sensor distance bias for sensors 6 and 5 in the non-ferrous rotation model under different interference conditions

Table 15 - Comparison of average baseline inter-sensor distance for sensors 6 and 5 with inter-sensor distance measured when interference sources were present

Trial condition	Sensors 6 and 5 (mm)	Bias (mm)	% difference
Baseline	9.240	------	------
EGG	9.258	0.018	0.189
EGG and retainer	9.256	0.016	0.170
EGG and palate expander	9.254	0.014	0.148
Retainer	9.256	0.016	0.168
Palate expander	9.256	0.016	0.170

Table 16 - Maximum error of the inter-sensor distance for the non-ferrous rotation model

Trial condition	Inter-sensor distance bias (mm)	Standard deviation (mm)	Maximum error (mm)
Baseline	0	0.073	0.073
EGG	0.018	0.061	0.079
EGG and retainer	0.016	0.063	0.079
EGG and palate expander	0.014	0.063	0.077
Retainer	0.016	0.063	0.079
Palate expander	0.016	0.063	0.079

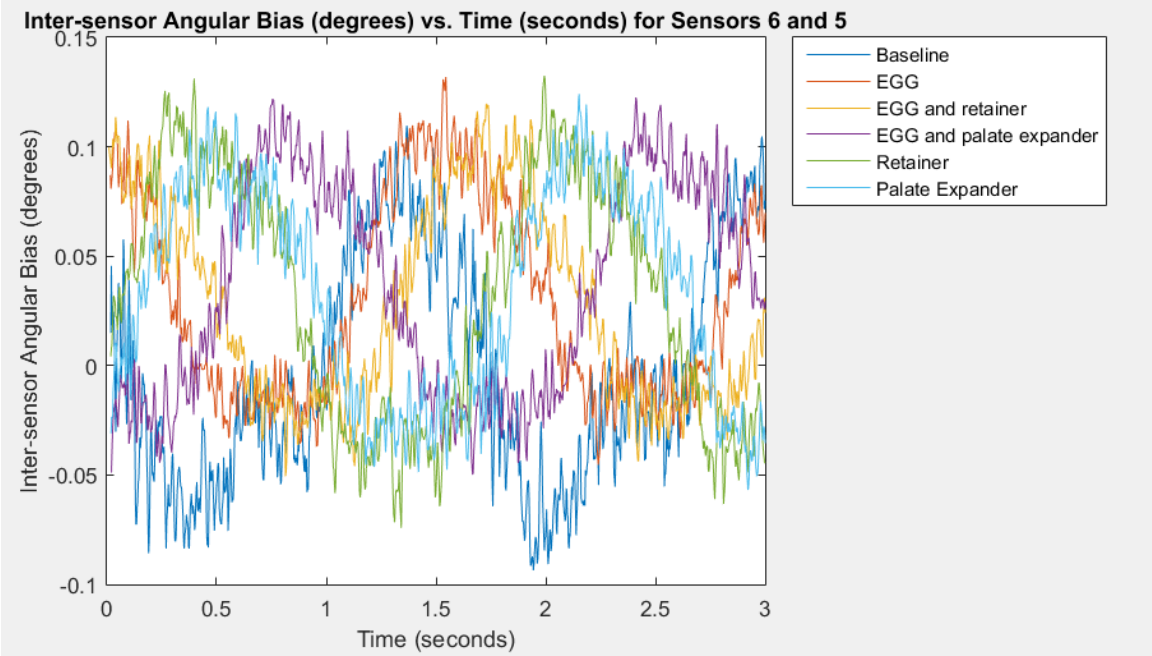

Figure 25 – Inter-sensor angular biases for sensors 6 and 5 in the non-ferrous rotation model with sources of interference present

Table 17 - Inter-sensor angle bias present with different interference conditions

Trial condition	Average inter-sensor angle (°)	Bias (°)	% difference
Baseline	67.799	------	------
EGG	67.835	0.036	0.053
EGG and retainer	67.833	0.034	0.051
EGG and palate expander	67.828	0.029	0.043
Retainer	67.825	0.027	0.039
Palate expander	67.826	0.027	0.040

Table 18 - Maximum error of sensors 6 and 5 for the non-ferrous rotation model

Trial condition	Inter-sensor angular bias (°)	Standard deviation (°)	Maximum error (°)
Baseline	0	0.051	0.051
EGG	0.036	0.047	0.083
EGG and retainer	0.034	0.049	0.083
EGG and palate expander	0.029	0.051	0.080
Retainer	0.027	0.053	0.080
Palate expander	0.027	0.049	0.076

5.5 Discussion

Table 14 shows the stationary standard deviation and measured value of the inter-sensor distance and angle. For both distance and angle, the standard deviation of the stationary baseline trial was lower than that of the moving baseline trial by a factor of 7 and 10 respectively. This indicates that the movement of the model added noise to the EMA signal, although it is still on a relatively low order of magnitude. The stationary baseline distance was 9.223 mm, which was 0.02 mm lower than the baseline distance measured while the model was moving. This suggests that bias is also added to the EMA measurements during sensor movement.

In both the inter-sensor distance and the inter-sensor angle trials, small periodic peaks can be observed for the duration of the trial (Figure 24 and Figure 25). Similar peaks were observed in the baseline trial (Figure 21). This supports the former hypothesis that the physical stress placed on the model caused additional movement to the model. The spikes would thus represent a physical flaw in the model instead of any error in the EMA system.

As seen in Table 16, the maximum error for inter-sensor distance is less than 0.1 mm, which is within the NDI error specification of 0.5 mm.

The maximum error for the baseline trial is lower than that of the other trials by about 0.006 mm at the most. This shows that any bias or noise caused by the presence of metal in the field did not have a significant impact on the measurements taken by the EMA sensors. The presence of orthodontia with the EGG did not significantly increase the error experienced by the system. The error measured when the EGG and palate expander were both present in the field was slightly lower than the error measured when either device was present individually.

Additionally, Table 18 shows that the maximum inter-sensor angular error is less than 0.1°. While there is no NDI specification to compare with this value, the low error indicates that the presence of metal did not strongly impact the orientation data. The measured inter-sensor angles were slightly higher with metal in the field, but the small difference of less than 0.1° could have resulted from the presence of a spike caused by a physical jerk of the model, and so is not conclusive. There did not seem to be any correlation between the amount of metal in the field and the standard deviation of the

inter-sensor angle. The standard deviation of the baseline inter-sensor angle is higher than that of the two trials when the EGG and palate expander were present, respectively.

With respect to the maximum error of both inter-sensor distance and inter-sensor angle, there was generally a higher maximum error when sources of interference were present. However, these errors still were well within the error specification of the NDI Wave system.

6. DETERMINATION OF EFFECTS OF ORIENTATION ON ACCURACY

6.1 Purpose

In clinical applications, the EMA sensors are not only moved with a nonzero velocity, but are also oriented in multiple ways as the articulators change position. Therefore, the interference experienced by the EMA system alone and by the EGG and EMA systems together was measured when the EMA sensors experienced a varying orientation with respect to the electromagnetic field.

In order to accomplish this, a model was created to rotate, rather than translate, the sensors so that the position and orientation accuracy could be examined as the sensor orientation was varied.

6.2 Construction of Model

The non-ferrous orientation model, shown below in Figure 26, was created using plastic pieces and a wooden cylinder. The wooden cylinder was hollowed at the ends to allow the plastic pieces to fit inside and thus rotate the model. The sensors were inserted into holes so that they would be positioned approximately at the axis of rotation and thus have minimal changes in position as the model rotated.

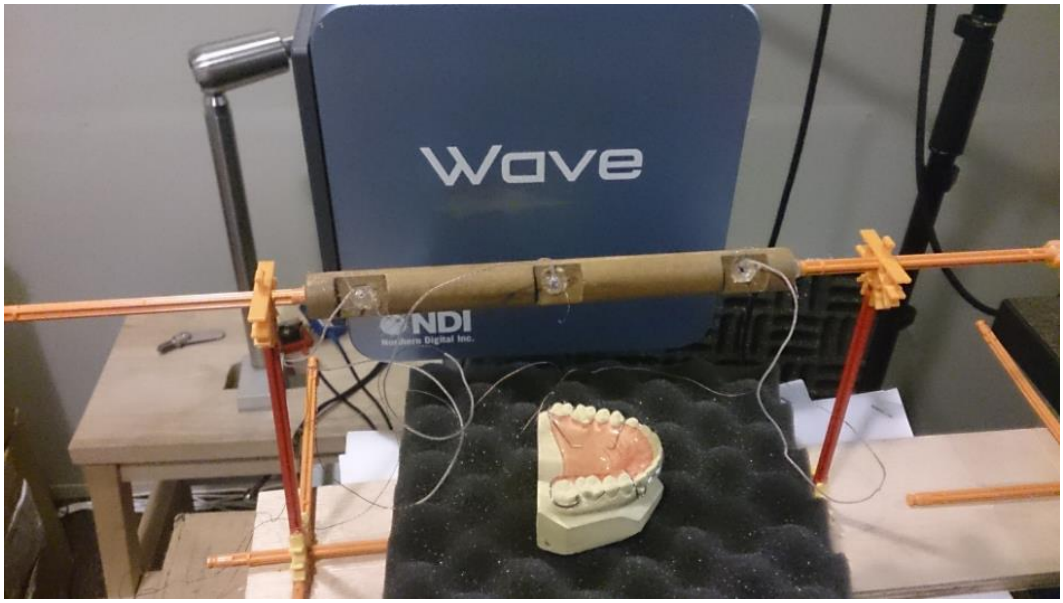

Figure 26 - Construction of the non-ferrous orientation model with palate expander

Figure 27 - Diagram of model and its movement

The diagram of the model shows that each sensor is located approximately on the radius of rotation. As a result, each sensor experiences identical rotational velocity with very little translational movement. The radius of the sensors' path is very small, with each sensor being approximately rotated in place.

The orthodontic appliances were placed beneath the wooden cylinder, while the EGG sensors were attached to a rolled rubber pad to simulate the attachment around the throat.

6.3 Data Collection

6.3.1 Methodology

The primary objective of the orientation model was to examine the effects of changing orientation on the accuracy of the EMA system. For each trial as the sensor orientation was changed, the EMA was rotated at the same speed – approximately 30 rpm. One physical limitation of the model was that the wires of the sensors experienced an increasing tensile force as each trial proceeded. The lower speed of 30 rpm enabled trial times of approximately seventeen seconds before the sensors experienced a force large enough to interfere with model behavior. It should be noted that the sensors would not be experiencing a full rotation in clinical situations.

For each trial, the model was rotated for approximately seventeen seconds. There were six trials in total, with each trial corresponding to a different interference condition: none/baseline, EGG, EGG and retainer, EGG and palate expander, retainer, and palate expander.

For each trial, the distance and angle between inter-sensor pairs were found. The zero-mean of the baseline data was found, and the average distance and inter-sensor angle from the baseline trial were subtracted from the distance and inter-sensor angle data of the other trials. This served to show the degree of the deviation from the baseline caused by each interference condition.

6.4 Results

There were three pairs of sensors from which data was analyzed: sensors 1 and 2, sensors 2 and 3, and sensors 1 and 3. The data presented below is from sensor pair

containing sensors 1 and 2. The data from the other sensor pairs is presented in Appendix C.

The biases present during each trial were calculated for the distance between sensors 1 and 2. Table 19 shows the value of the biases, which were found by subtracting the average baseline distance from the average distance of each trial. The variation in inter-sensor distance can be seen below in Figure 28.

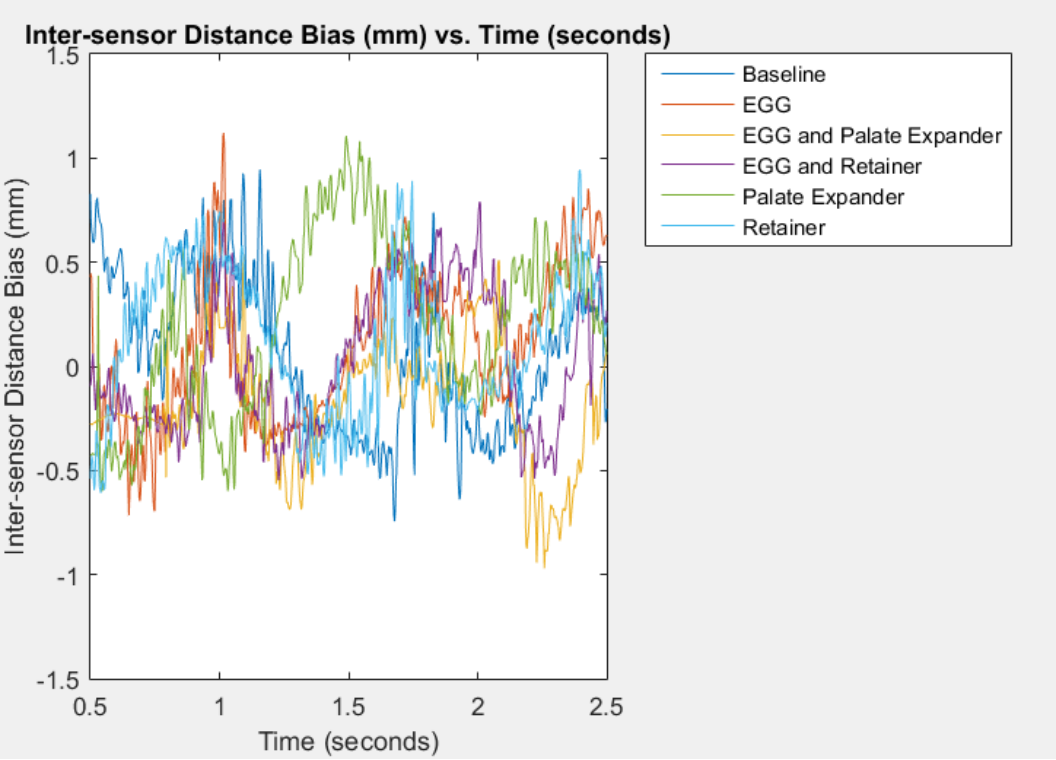

Figure 28 – Intser-sensor distance biases for sensors 1 and 2 in the non-ferrous orientation model

Table 19 – Inter-sensor distance bias present in trials of non-ferrous orientation model with different sources of interference were present

Trial	Average distance between Sensors 1 and 2 (mm)	Bias (mm)	% difference
Baseline	74.452	------	------
EGG	74.506	0.054	0.0724
EGG and Retainer	74.288	-0.164	-0.220
EGG and Palate Expander	74.249	-0.203	-0.273
Retainer	74.475	0.024	0.032
Palate Expander	74.573	0.121	0.162

The maximum error was calculated for each trial by adding the bias and standard deviation. Since the standard deviation is the deviation from the mean either in the positive or negative direction, it was assigned the same sign as the bias in order to find the maximum error.

Table 20 - Shows the maximum error present in each trial for the non-ferrous orientation model

Trial	Bias (mm)	Standard deviation (mm)	Maximum error (mm)
Baseline	0	0.323	0.323
EGG	0.054	0.352	0.406
EGG and Retainer	-0.164	0.373	-0.537
EGG and Palate Expander	-0.203	0.282	-0.485
Retainer	0.024	0.328	0.352
Palate Expander	0.121	0.412	0.533

The inter-sensor angle biases for sensors 1 and 2 were also calculated and are shown below in Table 21. The variation in the inter-sensor angle for each trial can be seen in Figure 29.

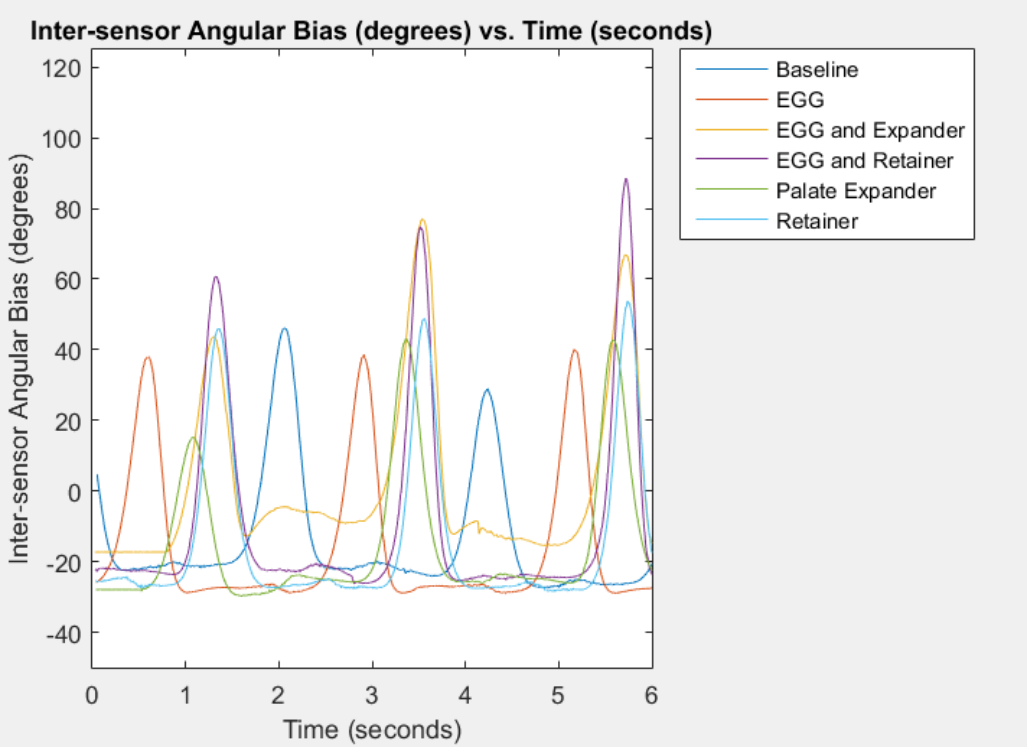

Figure 29 – Inter-sensor angular biases for sensors 1 and 2 present in the non-ferrous orientation model

Table 21 - Inter-sensor angular biases present for each trial of the non-ferrous orientation model

Trial	Sensors 1 and 2 (°)	Bias (°)	% difference
Baseline	55.085	-----	-----
EGG	38.766	-16.319	-29.625
EGG and Retainer	56.200	1.116	2.025
EGG and Palate Expander	46.176	-8.909	-16.174
Retainer	40.589	-14.496	-26.316
Palate Expander	40.173	-14.912	-27.070

Table 22 - Maximum inter-sensor angular error for each trial of the non-ferrous orientation model

Trial	Sensors 1 and 2 (°)	Standard deviation (°)	Maximum error
Baseline	0	27.520	27.520
EGG	-16.319	21.962	-38.281
EGG and Retainer	1.116	32.181	33.297
EGG and Palate Expander	-8.909	25.127	-34.036
Retainer	-14.496	23.977	-38.473
Palate Expander	-14.912	19.862	-34.774

6.5 Discussion

While there is no stationary baseline data for the non-ferrous orientation model, the baseline standard deviations of the inter-sensor distance and angle can be compared against those of the stationary non-ferrous rotation model. The stationary standard deviation for the baseline trial was 0.010 mm in the non-ferrous orientation model, the standard deviation was over 30 times higher at 0.323 mm. In addition, the standard deviation of the stationary baseline trial was 0.006°, while the standard deviation of the baseline trial of the non-ferrous orientation model was over 27°, higher by a factor of 4500. This indicates that error was introduced into the system by the rotation of the model and that the trials with metal present must be analyzed with regards to this introduced error.

Table 19 and Table 20 show the results of introducing metal into the electromagnetic field on the distance information gathered by the non-ferrous orientation model. As seen by Table 20, the maximum error for the trial with the palate expander and the trial containing the EGG and retainer exceeded the NDI Wave error specification of $\pm$0.5 mm. Additionally, the trial containing the EGG and palate expander was within 0.15 mm of exceeding the error specification. When examining Table 20, however, it is important to note that the baseline trial had a maximum error of 0.323 mm. This is higher than half of the error specification. In addition, the standard deviations did not appear to differ significantly among the trials, with the highest difference from the baseline value being 0.090 mm. The baseline standard deviation was higher than the standard deviation

in the trial in which the EGG and palate expander were present, and was within 0.005 mm of the trial in which the retainer was present.

The inter-sensor angular data for each trial also indicated high maximum error, as seen in Table 22, with the maximum error being close to 40° from the baseline value. However, it should be noted that the baseline trial again did not show a significantly lower standard deviation. While the maximum baseline error was lower, the standard deviation was higher than in every trial except the trial with the EGG and retainer present.

The large error values in both the baseline trial and the trials in which metal was present indicate that the presence of metal did not necessarily cause the error. The peaks in both the inter-sensor angle and inter-sensor distance data, as seen in Figure 28 and Figure 29, indicate that the error varied periodically with regards to the physical rotation of the model. Thus, the high error values cannot be attributed only to the presence of metal. Since the inter-sensor distance measurements that showed significant interference are only just outside the specified error and the standard deviation of the baseline trial is high, the physical model is most likely to blame for exceeding the error specification.

The inter-sensor angle data in Figure 29 shows peaks that appear to increase in amplitude as time increases. This is likely due to tension on the wires of the sensors, which may have slightly changed the orientation of the sensors. The sensors would no longer be rigidly attached, and so larger changes in inter-sensor angle would be observed as the trial continued.

In summary, although the inter-sensor distance and angle maximum errors are higher than seen in the non-ferrous rotation model and in some cases exceed the error

specification set by the NDI Wave system, the physical model likely contributed system error due to the sudden orientation change and tension on the sensors. Thus, it is still possible that the EMA system could be used with the EGG, retainer, and/or palate expander present in the field.

7. CONCLUSION

7.1 Summary

The objective of this research has been to identify whether the interference between the EGG and EMA systems is significant and, if so, to characterize it in such a way that the interference could be filtered out in post-processing software.

In order to accomplish this, initial data was first taken with a stationary bite plate in order to assess the degree of interference when the EGG was present. Data analysis showed that the interference present was insignificant, with the standard deviation of the inter-sensor distance being less within the error specification of $\pm$0.5 mm.

Since the articulators would be changing orientation and moving with variable speed while a subject spoke, this data was deemed to be insufficient to conclude that the EGG and EMA systems could be used concurrently. Two additional models were thus created: one which would move the sensors at varying speeds while maintaining constant orientation, and the other which would change the orientation of the sensors while maintaining constant speed. In addition to testing the EMA system by combining it with the EGG system, it was decided that orthodontic appliances would also be added in as a variable to test what effect they have on system accuracy. There were five different groupings that formed sources of interference for the trials: EGG, EGG with retainer, EGG with palate expander, retainer, and palate expander. A baseline trial in which no metal was present within the field was also conducted for each model.

The non-ferrous rotation model was created using plastic and contained a wooden platform where the sensors were rigidly attached. Different supply voltages were applied to the model so that the platform moved in a circular path at varying speeds. The

resulting data was analyzed for interference in both position and orientation data. The velocity of the data shown in this thesis was 122.511 mm/s, which is close to the maximum average articulator speed of 125 mm/s [22]. At this speed, the interference was not significantly present in the position or orientation data. With respect to the inter-sensor difference, the standard deviation of the distance from the average distance was within the error specification of $\pm$0.5 mm with each source of interference present. Although the orientation data does not have a stated error specification, the standard deviation for the different interference source cases was less than 0.5°, which should not have a significant bearing on the accuracy of the data interpretation in a clinical setting.

The non-ferrous orientation model was created using plastic and a wooden cylinder in which the sensors were rigidly attached. A constant voltage was applied to the model so that the wooden cylinder spun at a consistent speed around its center axis. The resulting data was then examined to determine the degree of interference present in the position and orientation data. Although the standard deviations of the inter-sensor distance were higher than those of the non-ferrous rotation model, the EMA still performed within the error specification for each source of interference. When examining the orientation data, however, the average standard deviation was higher than 20°. While this degree of inaccuracy could lead to false assumptions if occurring in clinical settings, it should be noted that the standard deviation of the trial containing no source of interference was also higher than 20°. Since it does not appear as though the orientation data varies significantly between the baseline and the trials with sources of interference, it can be concluded that the error is resulting from the system and not the presence of the EGG or orthodontia.

7.2 Contributions

Analysis of the data has supported the hypothesis that the presence of the EGG and orthodontic appliances did not cause significant interference in the data recorded by the EMA sensors. As a result, future studies of dysarthria can be conducted in which simultaneous articulator and vocal fold information can be collected from those suffering from dysarthria. This will help to characterize the motor speech issues, both laryngeal- and articulator-based, that accompany dysarthria. In addition, it will be possible for the EGG system to be used concurrently with the EMA system in order to synthesize a more natural-sounding voice that more closely resembles the voice quality of the subject through the use of the RASS system.

7.3 Future Work

While the experiments performed in this thesis indicate that the EMA and EGG systems can be used simultaneously, more research is needed in order to prove that the two can be used together in a clinical situation without interfering with each other. All of the data collections took place with attaching the EMA sensors to a flat inanimate surface, which does not reflect the anatomy of the human mouth. Attaching the EMA and EGG sensors to a subject in a clinical application would obtain a better analysis of the simultaneous use.

An example of one such clinical application would be using the EGG at the same time as an EMA while the EMA is being used to obtain a specific diagnosis or distinction. If the EMA system can perform this distinction while the EGG is in the field and attached to the subject, any error produced by the EGG must therefore be negligible enough that the two can be used together. Examining the statistics – the percentage of

false positives, false negatives, and correct diagnoses – would also be a way to characterize the usefulness of utilizing the systems together and determine if the two systems are better at characterization of speech signals together than either is separately.

8. REFERENCES

[1] T. Hain and E. Uraga, "Automatic Speech Recognition Experiments with Articulatory Data," in *Interspeech: ICSLP*, Pittsburgh, 2006.

[2] A. Kolb, "Software tools and analysis methods for the use of electromagnetic articulography data in speech research," Marquette University, Milwaukee, 2015.

[3] A. Kolb, "Use of an Electroglottograph to Drive an LF-Model-Based Speech Synthesizer," Marquette University, Milwaukee, 2014.

[4] D. Childers, D. M. Hicks, G. P. Moore and Y. A. Alaska, "A model for vocal fold vibratory motion, contact area, and the electroglottogram," *Journal of the Acoustical Society of America,* vol. 80, no. 5, pp. 1309-1320, 1986.

[5] A. Behrman and R. F. Orlikoff, "Instrumentation in Voice Assessment and Treatment: What's the Use?," *American Journal of Speech-Language Pathology,* vol. 6, no. 4, pp. 9-16, 1997.

[6] B. H. Story, "Phrase-level speech simulation with an airway modulation model of speech production," *Comput Speech Lang.,* vol. 27, no. 4, pp. 989-1010, 2013.

[7] Y. Yunusova, J. R. Green and A. Mefferd, "Accuracy Assessment for AG500, Electromagnetic Articulograph," *Journal of Speech, Language, and Hearing Research,* vol. 52, pp. 547-555, 2009.

[8] A. Zierdt, "EMA and the Crux of Calibration," in *ICPhS*, Saarbrucken, 2007.

[9] "Wave User Guide," NDI, 2011.

[10] J. S. Perkell, M. H. Cohen, M. A. Svirsky, M. L. Matthies, I. Garabieta and M. T. T. Jackson, "Electromagnetic midsagittal articulometer systems for transducing speech articulatory movements," *J. Acoust. Soc. Am.,* vol. 92, no. 6, pp. 3078-3096, 1992.

[11] J. Berry, "Accuracy of the NDI Wave speech research system," *Journal of Speech, Language, and Hearing Research,* vol. 54, pp. 1295-1301, 2011.

[12] J. R. Westbury, J. Dembowski and G. Turner, "X-RAY MICROBEAM SPEECH PRODUCTION DATABASE USER'S HANDBOOK," Waisman Center on Mental Retardation & Human Development, University of Wisconsin, Madison, 1994.

[13] C. J. Bartle, J. V. Goozee, D. Scott, B. E. Murdoch and M. Kuruvilla, "EMA assessment of tongue-jaw co-ordination during speech in dysarthria following traumatic brain injury," *Brain Injury,* vol. 20, no. 5, pp. 529-545, 2006.

[14] J. Beskow, "Talking Heads: Models and Applications for Multimodal Speech Synthesis," KTH, Stockholm, 2003.

[15] A. Zierdt, P. Hoole and H. G. Tillman, "Development of a system for three-dimensional fleshpoint measurement of speech movements," in *Proceedings of the XIVth International Congress of Phonetic Sciences*, San Francisco, CA, 1999.

[16] S. Narayanan, E. Bresch, P. Ghosh, L. Goldstein, A. Katsamanis, Y. Kim, A. Lammert, M. Proctor, V. Ramanarayanan and Y. Zhu, "A Multimodal Real-Time MRI Articulatory Corpus for Speech Research," in *Interspeech*, Florence, 2011.

[17] D. H. Whalen, K. Iskarous, M. K. Tiede and D. J. Ostry, "A combined ultrasound/Optotrak measurement system for speech kinematics," in *6th International Seminar on Speech Production*, Sydney, 2003.

[18] A. J. Hanson, Visualizing Quaternions: series in Interactive 3D Technology, San Francisco: Morgan Kaufmann Publishers, 2006.

[19] M. Rothenberg and J. J. Mahshie, "MONITORING VOCAL FOLD ABDUCTION THROUGH VOCAL FOLD CONTACT AREA," *Journal of Speech and Hearing Research,* vol. 31, pp. 338-351, 1988.

[20] D. G. Childers, D. M. Hicks, G. P. Moore, L. Eskenazi and A. L. Lalwani, "Electroglottography and Vocal Fold Physiology," *Journal of Speech and Hearing Research,* vol. 33, pp. 245-254, 1990.

[21] S. M. Tasko and J. R. Westbury, "Speed-curvature relations for speech-related articulatory movement," *Journal of Phonetics,* vol. 32, pp. 65-80, 2004.

[22] D. Bauer, J. Kannampuzha, P. Hoole and B. J. Kroger, "Gesture Duration and Articulator Velocity in Plosive-Vowel-Transitions," in *COST 2102 Int. Training school 2009*, Berlin, 2010.

[23] F. L. Markley, Y. Cheng, J. L. Crassidis and Y. Oshman, "Averaging Quaternions".

9. APPENDICES

A. Initial Data Collection

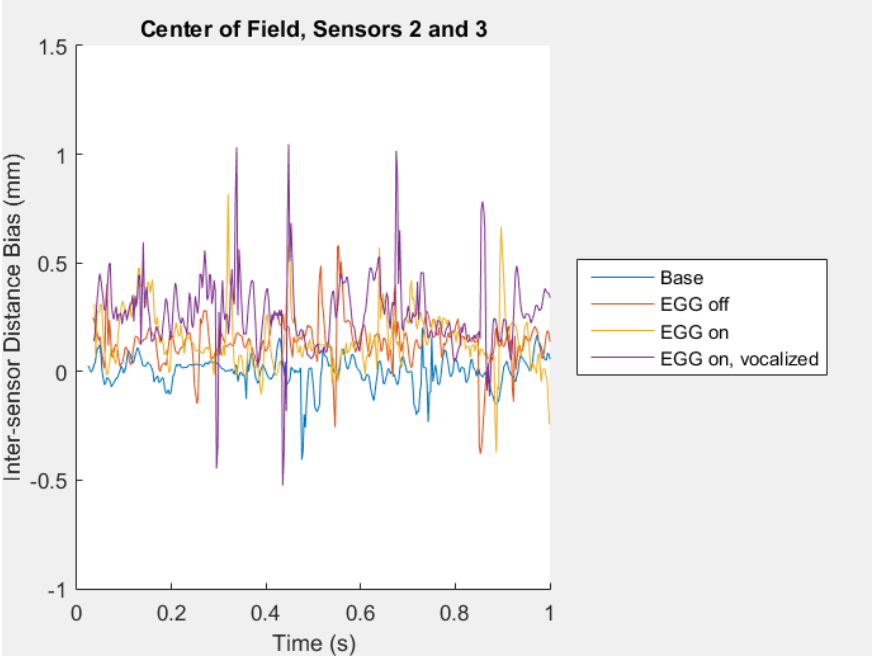

Figure 30 - Inter-sensor bias for sensors 2 and 3 in stationary trials

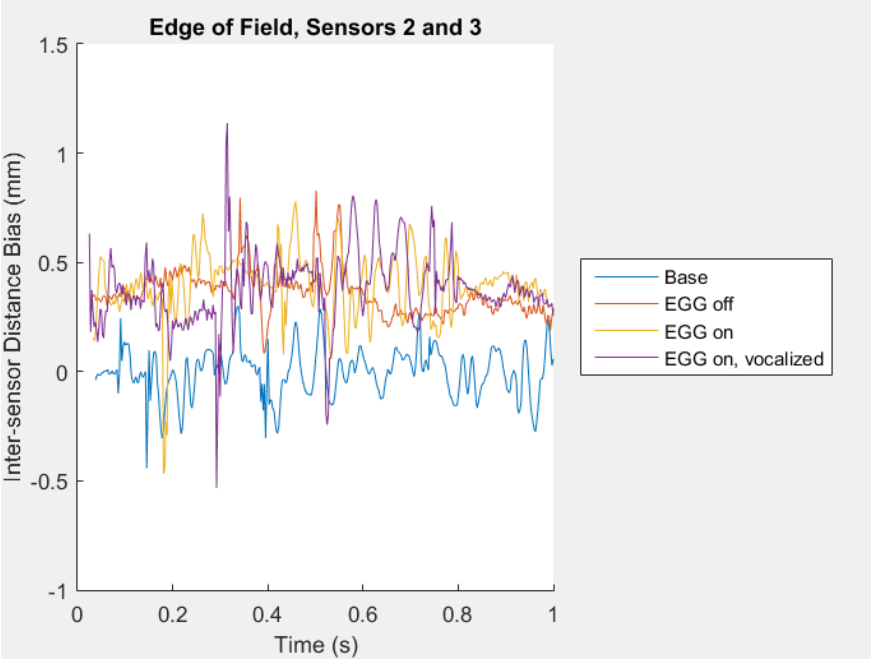

Figure 31 - Inter-sensor distance bias for sensors 2 and 3 in stationary trials

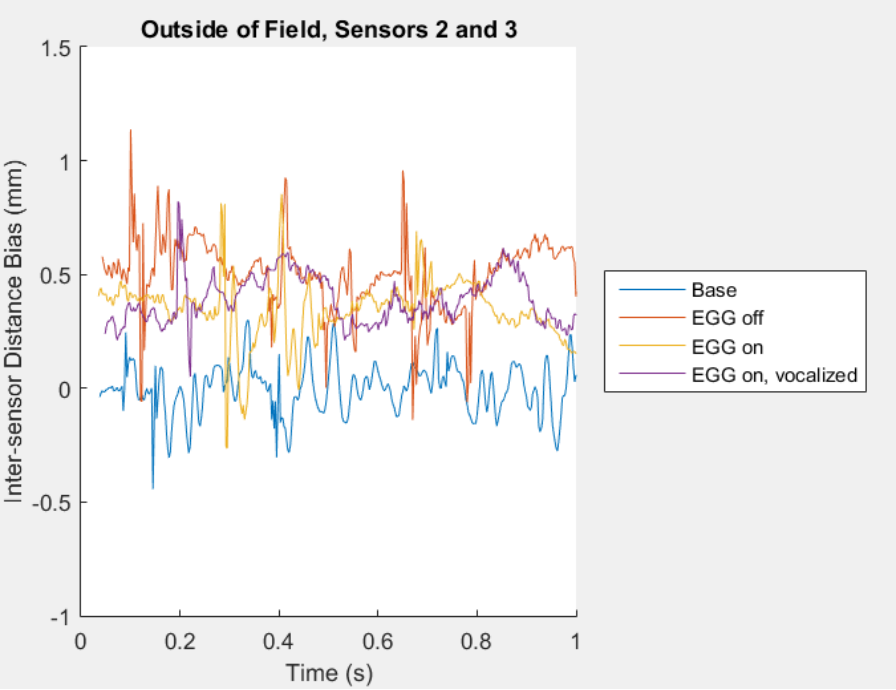

Figure 32 - Inter-sensor distance bias for sensors 2 and 3 in stationary trials

Table 23 - Comparison of average baseline inter-sensor distance with average inter-sensor distance of each interference trial at center of field for sensors 2 and 3

Trial condition (center)	Inter-sensor distance (mm)	Bias (mm)	% difference
Baseline	18.206	------	------
EGG off	18.343	0.137	0.751
EGG on, unvocalized	18.353	0.147	0.805
EGG vocalized	18.476	0.270	1.485

Table 24 - Comparison of average baseline inter-sensor distance with average inter-sensor distance of each interference trial at edge of field for sensors 2 and 3

Trial condition (edge)	Inter-sensor distance (mm)	Bias (mm)	% difference
Baseline	18.005	------	------
EGG off	18.365	0.360	2.000
EGG on, unvocalized	18.398	0.393	2.184
EGG vocalized	18.387	0.382	2.120

Table 25 - Comparison of average baseline inter-sensor angle with average inter-sensor angle of each interference trial when EGG sensors were outside of field for sensors 2 and 3

Trial condition (outside)	Inter-sensor distance (mm)	Bias (mm)	% difference
Baseline	18.005	-----	------
EGG off	18.509	0.504	2.800
EGG on, unvocalized	18.348	0.330	1.904
EGG vocalized	18.394	0.389	2.161

Table 26 - Maximum error when systems are stationary and present in center of field

	Bias (mm)	Standard deviation (mm)	Maximum error (mm)
Baseline	0	0.071	0.071
EGG off	0.137	0.104	0.241
EGG on, unvocalized	0.147	0.136	0.283
EGG on, vocalized	0.270	0.168	0.438

Table 27 - Maximum error when systems are stationary and present at edge of field

	Bias (mm)	Standard deviation (mm)	Maximum error (mm)
Baseline	0	0.113	0.113
EGG off	0.360	0.104	0.464
EGG on, unvocalized	0.393	0.193	0.586
EGG on, vocalized	0.382	0.165	0.547

Table 28 - Maximum error when systems are stationary, the EGG sensors are outside of the field, and the EMA sensors are at the edge of the field

	Bias (mm)	Standard deviation (mm)	Maximum error (mm)
Baseline	0	0.113	0.113
EGG off	0.504	0.157	0.661
EGG on, unvocalized	0.330	0.135	0.465
EGG on, vocalized	0.389	0.106	0.495

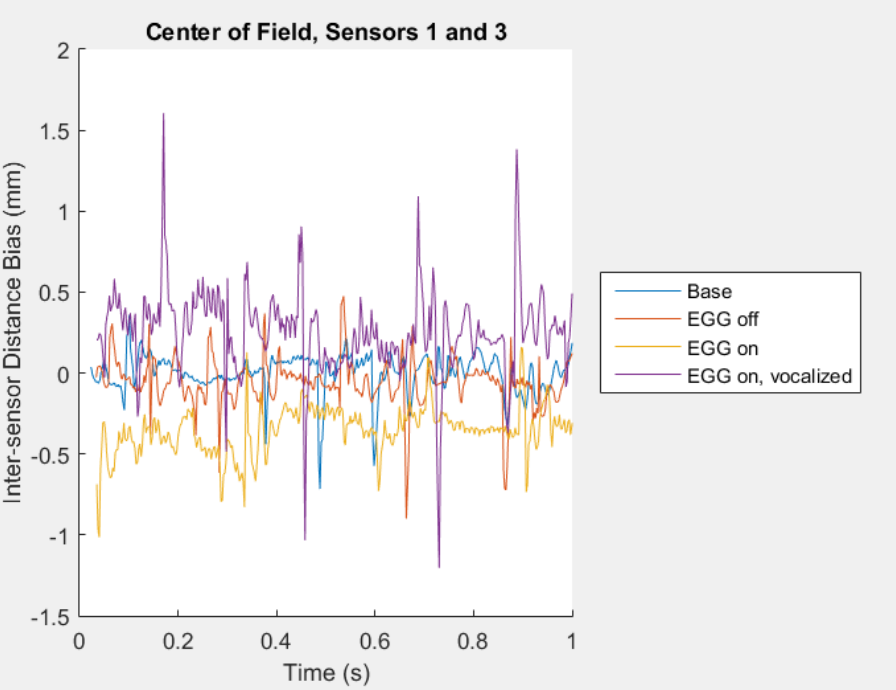

Figure 33 - Inter-sensor distance bias for sensors 1 and 3 in stationary trials

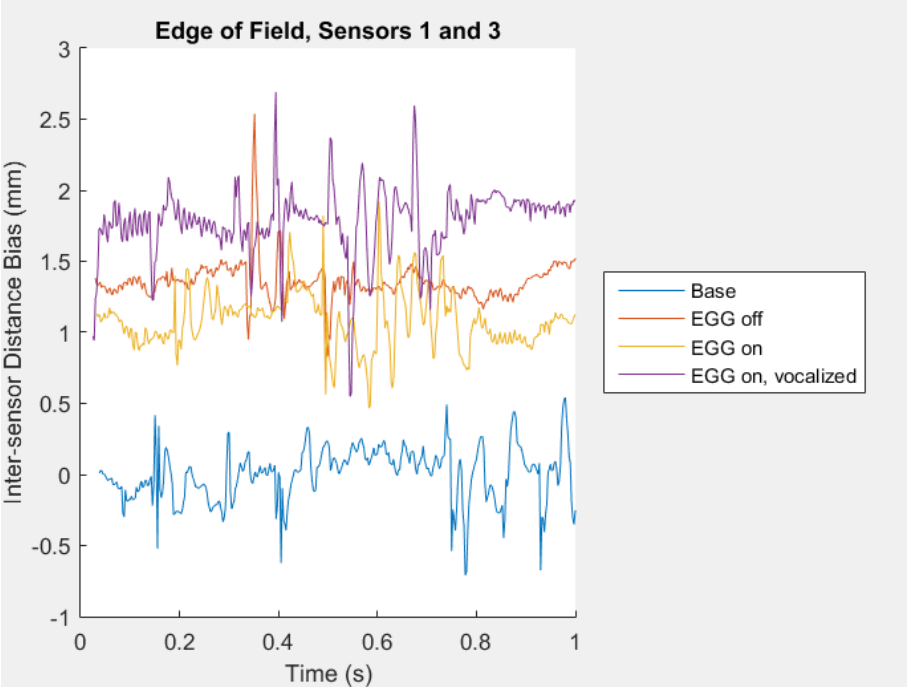

Figure 34 - Inter-sensor distance bias for sensors 1 and 3 in stationary trials

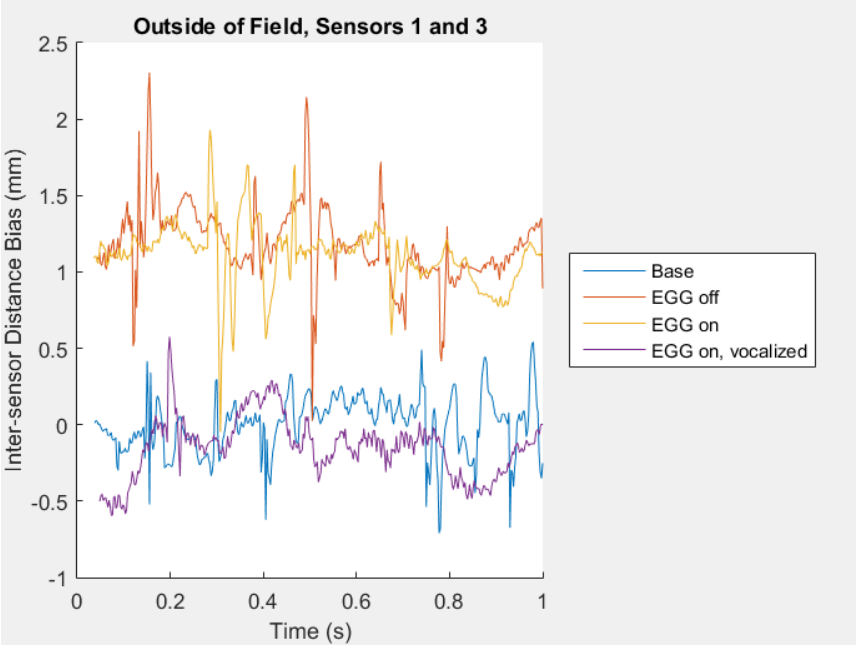

Figure 35 - Inter-sensor distance bias for sensors 1 and 3 in stationary trials

The biases and standard deviations for each trial were calculated and can be seen below.

Table 29 - Comparison of average baseline inter-sensor distance with average inter-sensor distance of each interference trial at center of field for sensors 1 and 3

Trial condition (center)	Inter-sensor distance (mm)	Bias (mm)	% difference
Baseline	32.175	------	------
EGG off	32.119	-0.056	-0.174
EGG on, unvocalized	31.817	-0.357	-1.111
EGG vocalized	32.430	0.256	0.795

Table 30 - Comparison of average baseline inter-sensor distance with average inter-sensor distance of each interference trial at edge of field for sensors 1 and 3

Trial condition (edge)	Inter-sensor distance (mm)	Bias (mm)	% difference
Baseline	30.747	------	------
EGG off	32.106	1.359	4.419
EGG on, unvocalized	31.830	1.083	3.521
EGG vocalized	32.531	1.784	5.803

Table 31 - Comparison of average baseline inter-sensor distance with average inter-sensor distance of each interference trial when EGG sensors were outside of field

Trial condition (outside)	Inter-sensor distance (mm)	Bias (mm)	% difference
Baseline	18.705	-----	------
EGG off	19.306	0.601	3.214
EGG on, unvocalized	19.297	0.593	3.169
EGG vocalized	18.371	-0.334	-1.783

Table 32 - Maximum error when systems are stationary and present in center of field

	Bias (mm)	Standard deviation (mm)	Maximum error (mm)
Baseline	0	0.119	-0.119
EGG off	-0.056	0.149	-0.205
EGG on, unvocalized	-0.357	0.155	-0.512
EGG on, vocalized	0.256	0.261	0.517

Table 33 - Maximum error when systems are stationary and present at edge of field

	Bias (mm)	Standard deviation (mm)	Maximum error (mm)
Baseline	0	0.191	0.191
EGG off	1.359	0.139	1.498
EGG on, unvocalized	1.083	0.193	1.276
EGG on, vocalized	1.784	0.191	1.975

Table 34 - Maximum error when systems are stationary, the EGG sensors are outside of the field, and the EMA sensors are at the edge of the field

	Bias (mm)	Standard deviation (mm)	Maximum error (mm)
Baseline	0	0.191	0.191
EGG off	0.601	0.250	0.851
EGG on, unvocalized	0.593	0.207	0.800
EGG on, vocalized	-0.334	0.198	-0.532

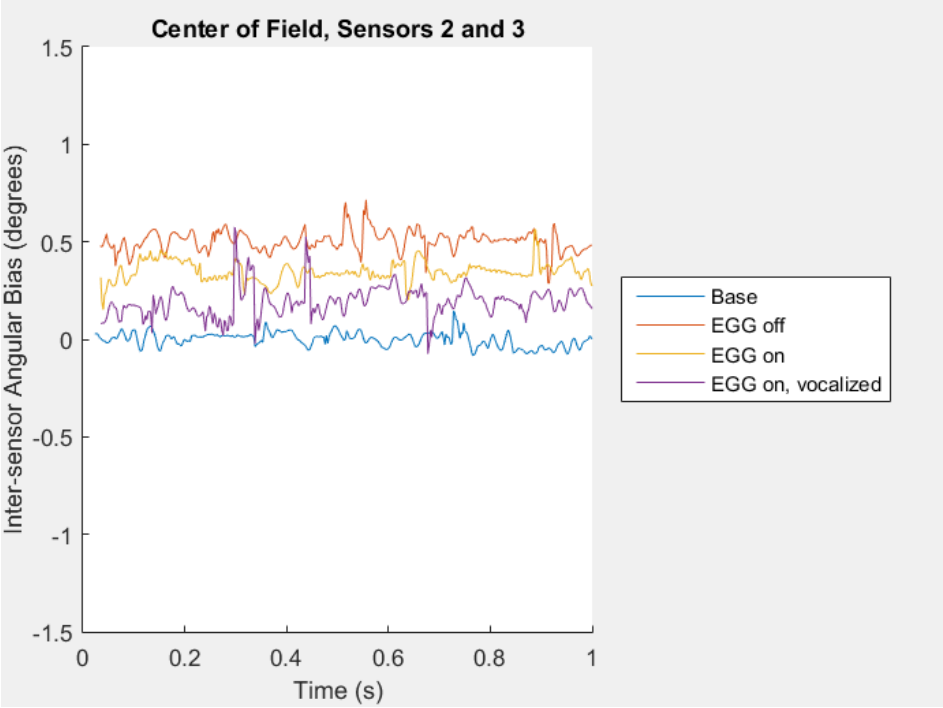

Figure 36 – Inter-sensor angular biases present between sensors 2 and 3 in the center of the field for the stationary trials

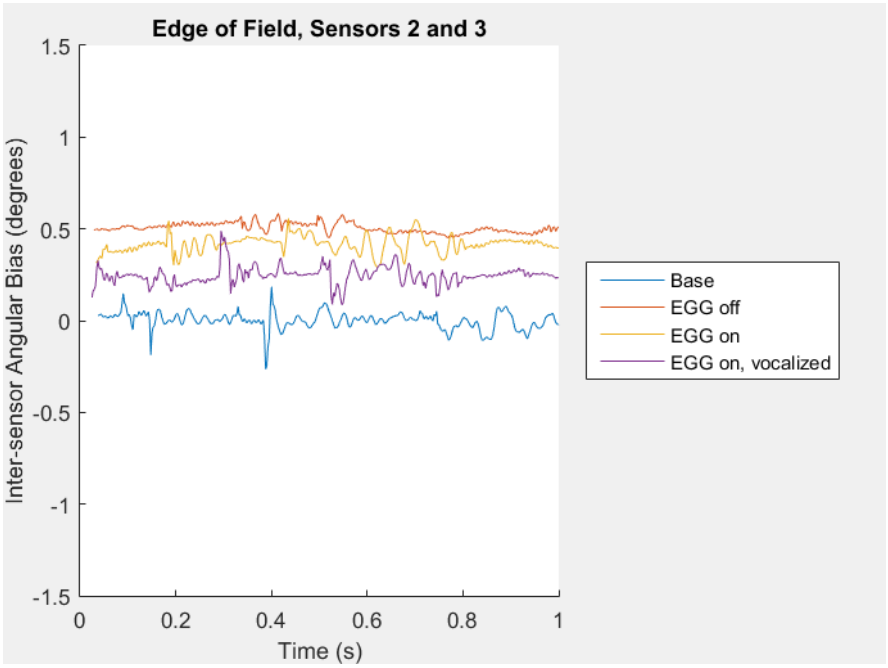

Figure 37 – Inter-sensor angular biases present between sensors 2 and 3 at the edge of the field for the stationary trials

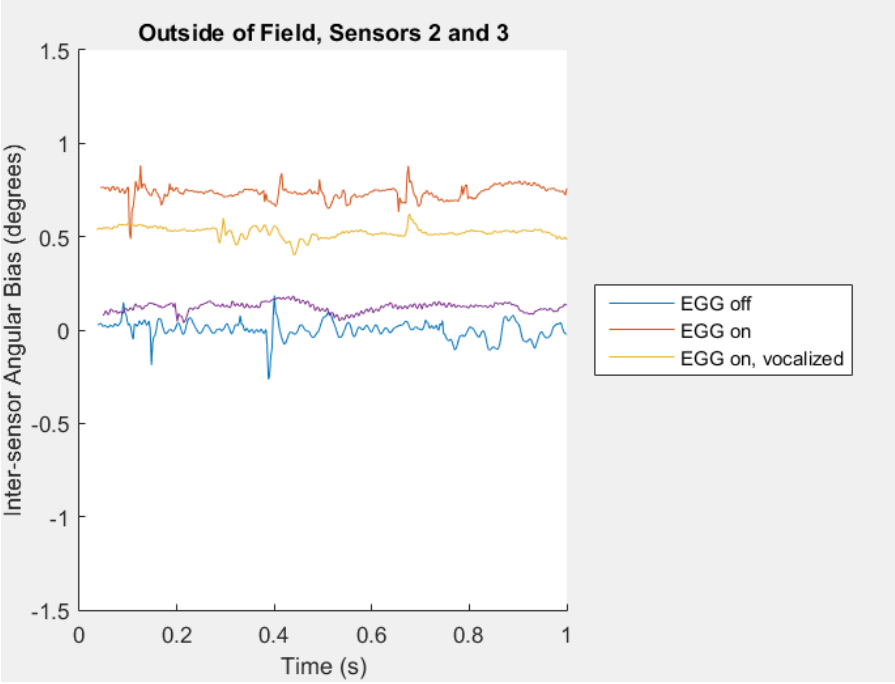

Figure 38 - Angular biases present between sensors 2 and 3 with the EGG outside of the field for the stationary trials

Table 35 - Comparison of average baseline inter-sensor angle with average inter-sensor angle of each interference trial at center of field for sensors 2 and 3

Trial condition (center)	Inter-sensor angle (°)	Bias (°)	% difference
Baseline	26.326	------	------
EGG off	26.830	0.504	1.916
EGG on, unvocalized	26.672	0.346	1.314
EGG vocalized	26.518	0.192	0.729

Table 36 - Comparison of average baseline inter-sensor angle with average inter-sensor angle of each interference trial at edge of field for sensors 2 and 3

Trial condition (edge)	Inter-sensor angle (°)	Bias (°)	% difference
Baseline	26.101	-----	------
EGG off	26.607	0.506	1.938
EGG on, unvocalized	26.518	0.417	1.599
EGG vocalized	26.347	0.246	0.943

Table 37 - Comparison of average baseline inter-sensor angle with average inter-sensor angle of each interference trial when EGG sensors were outside of field for sensors 2 and 3

Trial condition (outside)	Inter-sensor angle (°)	Bias (°)	% difference
Baseline	26.101	-----	------
EGG off	26.938	0.737	2.824
EGG on, unvocalized	26.624	0.523	2.005
EGG vocalized	26.224	0.123	0.471

Table 38 - Maximum error when systems are stationary and present in center of field for sensors 2 and 3

	Bias (°)	Standard deviation (°)	Maximum error (°)
Baseline	0	0.036	0.036
EGG off	0.504	0.052	0.557
EGG on, unvocalized	0.346	0.051	0.397
EGG on, vocalized	0.192	0.077	0.269

Table 39 - Maximum error when systems are stationary and present at edge of field for sensors 2 and 3

	Bias (°)	Standard deviation (°)	Maximum error (°)
Baseline	0	0.047	0.047
EGG off	0.506	0.027	0.533
EGG on, unvocalized	0.417	0.045	0.462
EGG on, vocalized	0.246	0.049	0.295

Table 40 - Maximum error when systems are stationary, the EGG sensors are outside of the field, and the EMA sensors are at the edge of the field for sensors 2 and 3

	Bias (°)	Standard deviation (°)	Maximum error (°)
Baseline	0	0.047	0.047
EGG off	0.737	0.038	0.775
EGG on, unvocalized	0.523	0.028	0.551
EGG on, vocalized	0.123	0.025	0.148

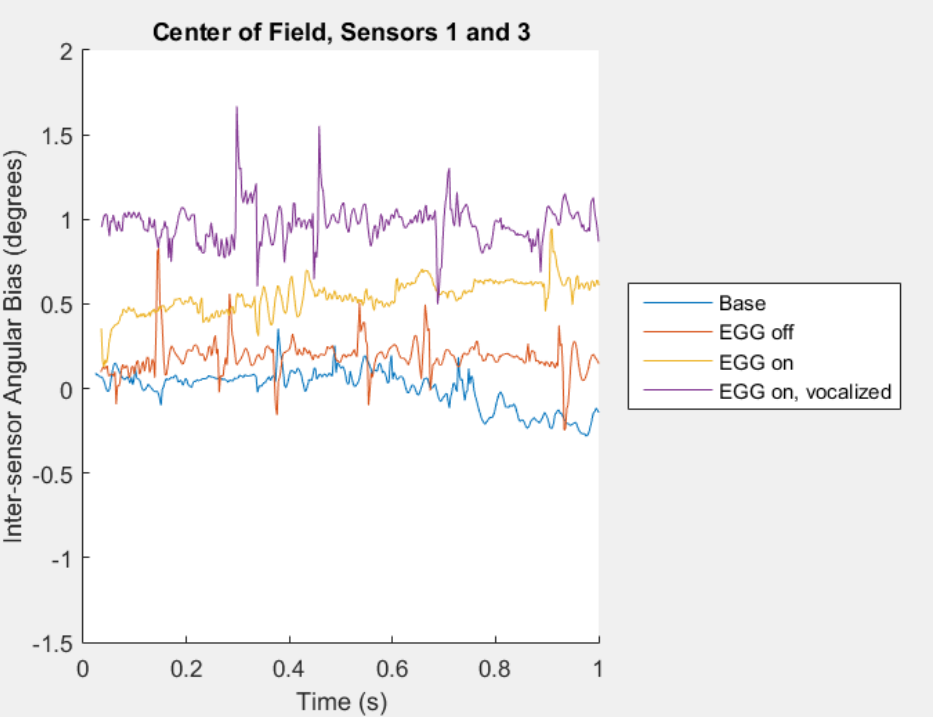

Figure 39 - Inter-sensor angular biases present between sensors 1 and 3 in the center of the field for the stationary trials

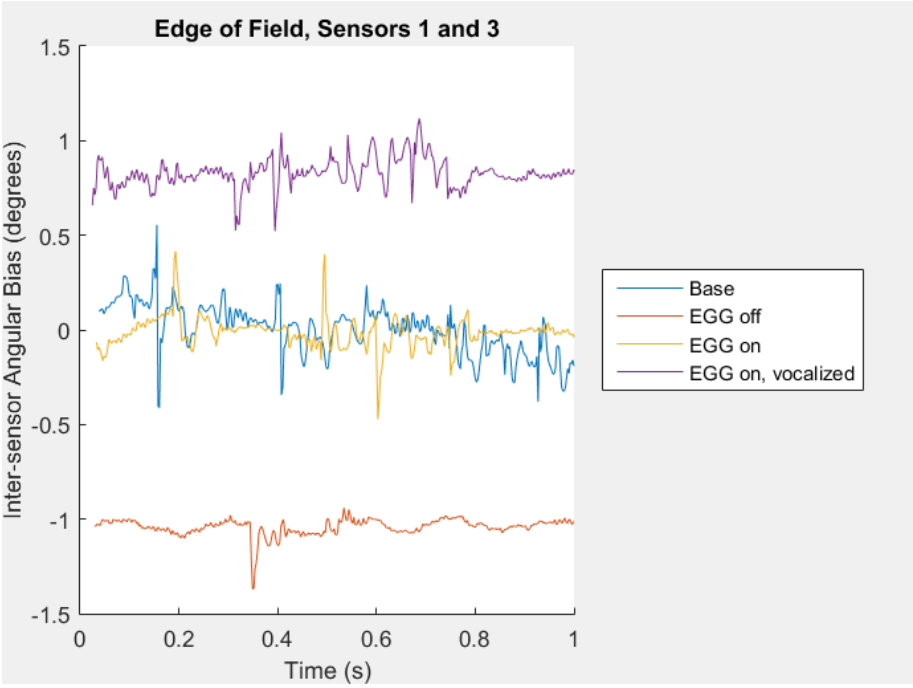

Figure 40 - Inter-sensor angular biases present between sensors 1 and 3 at the edge of the field for the stationary trials

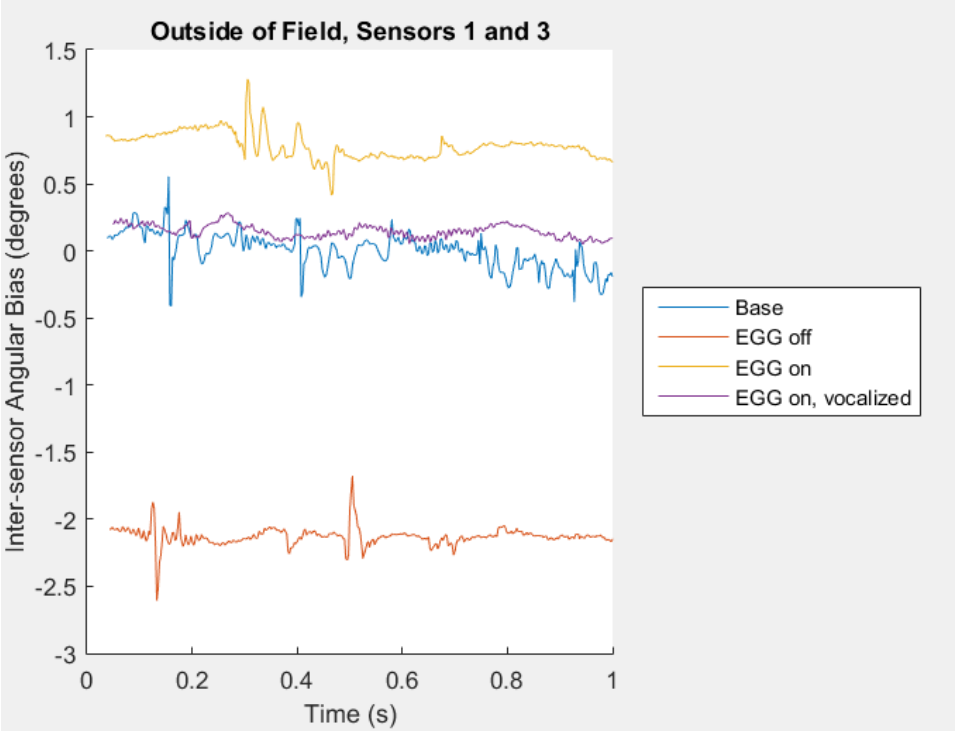

Figure 41 - Inter-sensor angular biases present between sensors 1 and 3 with the EGG outside of the field for the stationary trials

Table 41 - Comparison of average baseline inter-sensor angle with average inter-sensor angle of each interference trial at center of field for sensors 1 and 3

Trial condition (center)	Inter-sensor angle (°)	Bias (°)	% difference
Baseline	45.274	-----	------
EGG off	46.461	0.186	0.411
EGG on, unvocalized	45.820	0.545	1.204
EGG vocalized	46.249	0.975	2.152

Table 42 - Comparison of average baseline inter-sensor angle with average inter-sensor angle of each interference trial at edge of field for sensors 1 and 3

Trial condition (edge)	Inter-sensor angle (°)	Bias (°)	% difference
Baseline	44.504	------	------
EGG off	43.463	-1.041	-2.339
EGG on, unvocalized	44.489	-0.015	-0.034
EGG vocalized	45.332	0.828	1.861

Table 43 - Comparison of average baseline inter-sensor angle with average inter-sensor angle of each interference trial when EGG sensors were outside of field for sensors 1 and 3

Trial condition (outside)	Inter-sensor angle (°)	Bias (°)	% difference
Baseline	44.504	------	------
EGG off	42.375	-2.130	-4.784
EGG on, unvocalized	45.288	0.784	1.762
EGG vocalized	44.650	0.146	0.328

Table 44 - Maximum error when systems are stationary and present in center of field for sensors 1 and 3

	Bias (°)	Standard deviation (°)	Maximum error (°)
Baseline	0	0.113	0.113
EGG off	0.186	0.100	0.286
EGG on, unvocalized	0.545	0.103	0.648
EGG on, vocalized	0.975	0.115	1.090

Table 45 - Maximum error when systems are stationary and present at edge of field for sensors 1 and 3

	Bias (°)	Standard deviation (°)	Maximum error (°)
Baseline	0	0.136	0.136
EGG off	-1.041	0.043	-1.084
EGG on, unvocalized	-0.015	0.080	-0.095
EGG on, vocalized	0.828	0.077	0.905

Table 46 - Maximum error when systems are stationary, the EGG sensors are outside of the field, and the EMA sensors are at the edge of the field for sensors 1 and 3

	Bias (°)	Standard deviation (°)	Maximum error (°)
Baseline	0	0.136	0.136
EGG off	-2.130	0.067	-2.063
EGG on, unvocalized	0.784	0.100	0.884
EGG on, vocalized	0.146	0.049	0.195

B. Lego model

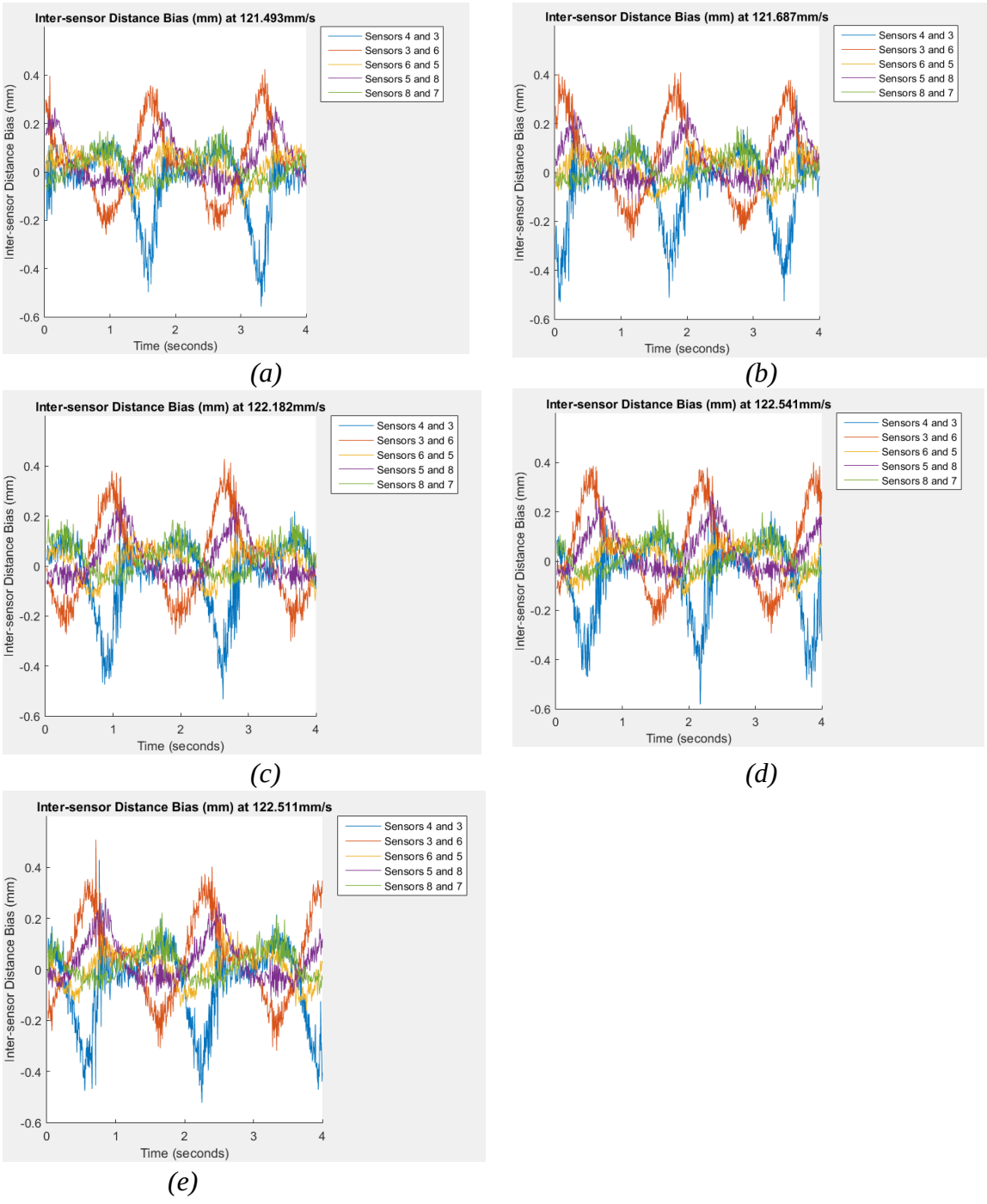

Figure 42 – Distance biases measured with the non-ferrous rotation model while experiencing different sources of interference

Figure 42(a) represents the inter-sensor distance bias while the EMA sensors were in the field with the EGG. Figure 42(b) represents the inter-sensor distance bias while both the EGG and retainer were present. Figure 42(c) represents the inter-sensor distance bias while both the EGG and palate expander were present. Figure 42(d) represents the inter-sensor distance bias while the retainer was present. Figure 42(e) represents the inter-sensor distance bias while the palate expander was present.

Table 47 - Standard deviation of inter-sensor distances for the non-ferrous rotation model

Trial condition	Sensors 4 and 3 (mm)	Sensors 3 and 6 (mm)	Sensors 6 and 5 (mm)	Sensors 5 and 8 (mm)	Sensors 8 and 7 (mm)
Baseline	0.1144	0.1008	0.0731	0.0566	0.0526
EGG	0.1411	0.1488	0.0611	0.0872	0.0585
EGG and retainer	0.1508	0.1563	0.0633	0.0862	0.0578
EGG and palate expander	0.1473	0.1574	0.0629	0.0889	0.0606
Retainer	0.1466	0.1538	0.0634	0.0865	0.0594
Palate expander	0.1470	0.1536	0.0628	0.0881	0.0591

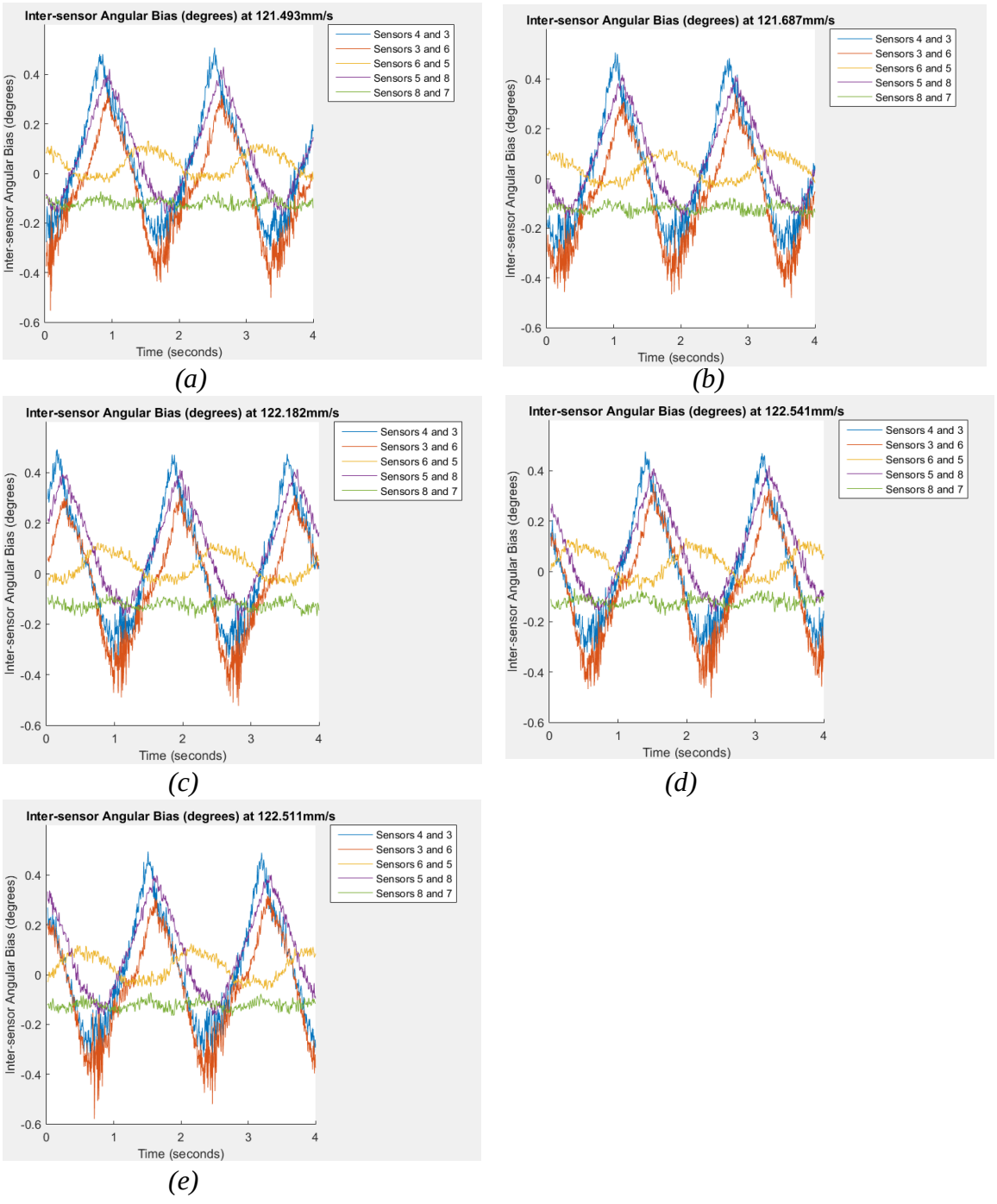

Figure 43 – Inter-sensor angular bias of the non-ferrous rotation model with sources of interference present

Figure 43(a) represents the inter-sensor angular bias while the EMA sensors were in the field with the EGG. Figure 43(b) represents the inter-sensor angular bias while both the

EGG and retainer were present. Figure 43(c) represents the inter-sensor angular bias while both the EGG and palate expander were present. Figure 43(d) represents the inter-sensor angular bias while the retainer was present. Figure 43(e) represents the inter-sensor angular bias while the palate expander was present.

Table 48 - Standard deviation of inter-sensor angles for the non-ferrous rotation model

Trial condition	Sensors 4 and 3 (°)	Sensors 3 and 6 (°)	Sensors 6 and 5 (°)	Sensors 5 and 8 (°)	Sensors 8 and 7 (°)
Baseline	0.1708	0.1656	0.0514	0.1520	0.0236
EGG	0.2177	0.2006	0.0469	0.1673	0.0156
EGG and retainer	0.2217	0.2058	0.0485	0.1663	0.0159
EGG and palate expander	0.2208	0.2088	0.0506	0.1689	0.0159
Retainer	0.2182	0.2071	0.0530	0.1660	0.0167
Palate expander	0.2208	0.2046	0.0493	0.1671	0.0158

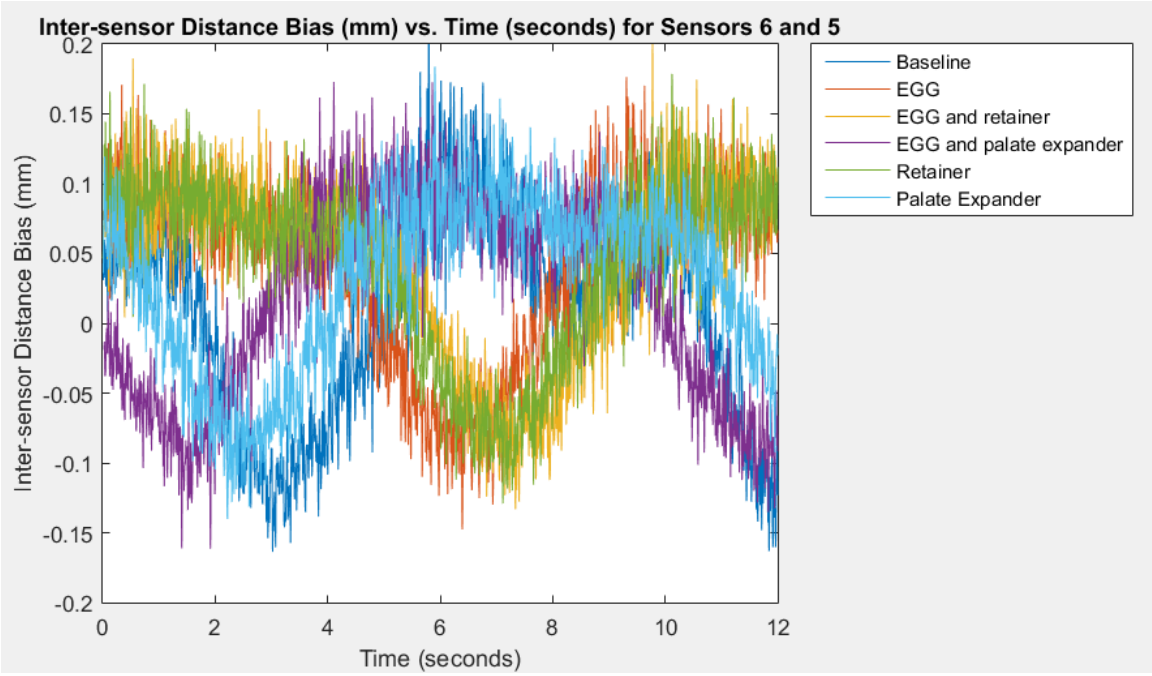

Figure 44 - Inter-sensor distances biases for sensors 6 and 5 at approximately 25mm/s in the non-ferrous rotation model at approximately 25 mm/s

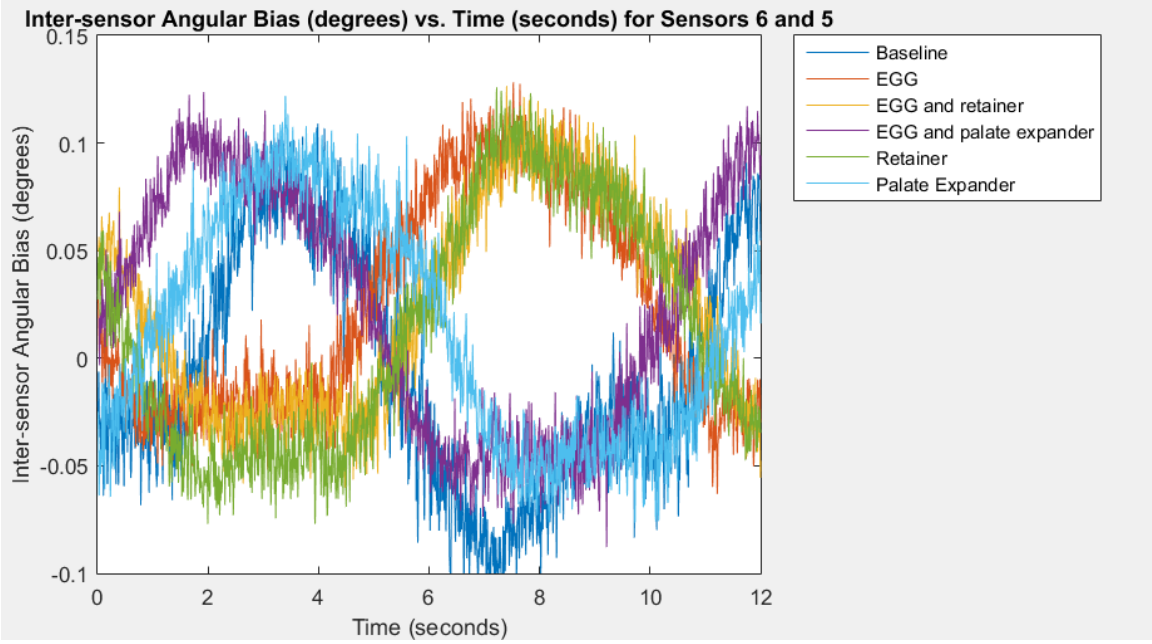

Figure 45 - Inter-sensor angular biases for sensors 6 and 5 in the non-ferrous rotation model at approximately 25 mm/s

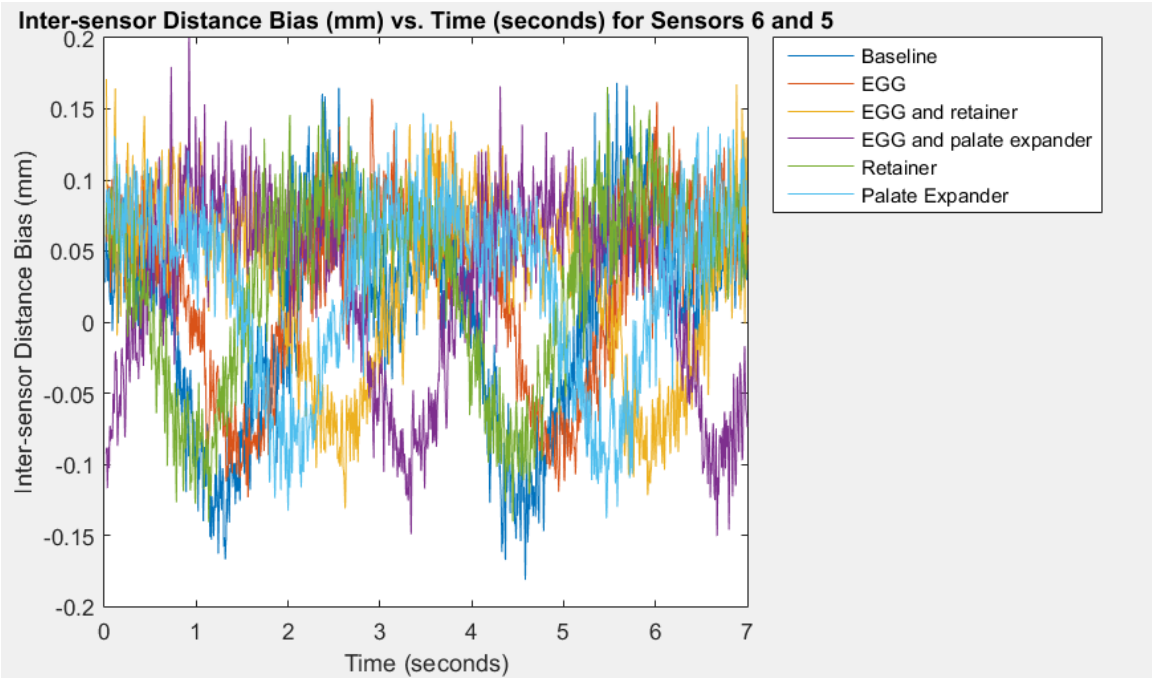

Figure 46 - Inter-sensor distance biases for sensors 6 and 5 in the non-ferrous rotation model at approximately 65 mm/s

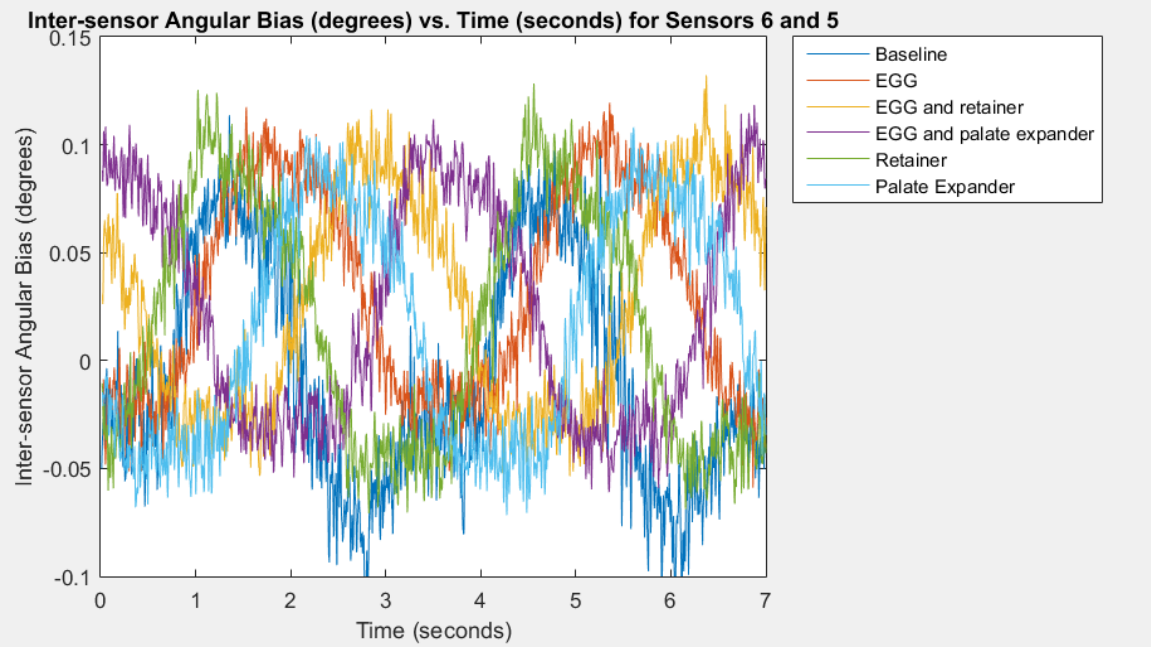

Figure 47 - Inter-sensor angular biases for sensors 6 and 5 in the non-ferrous rotation model at approximately 65 mm/s

C. Lincoln log

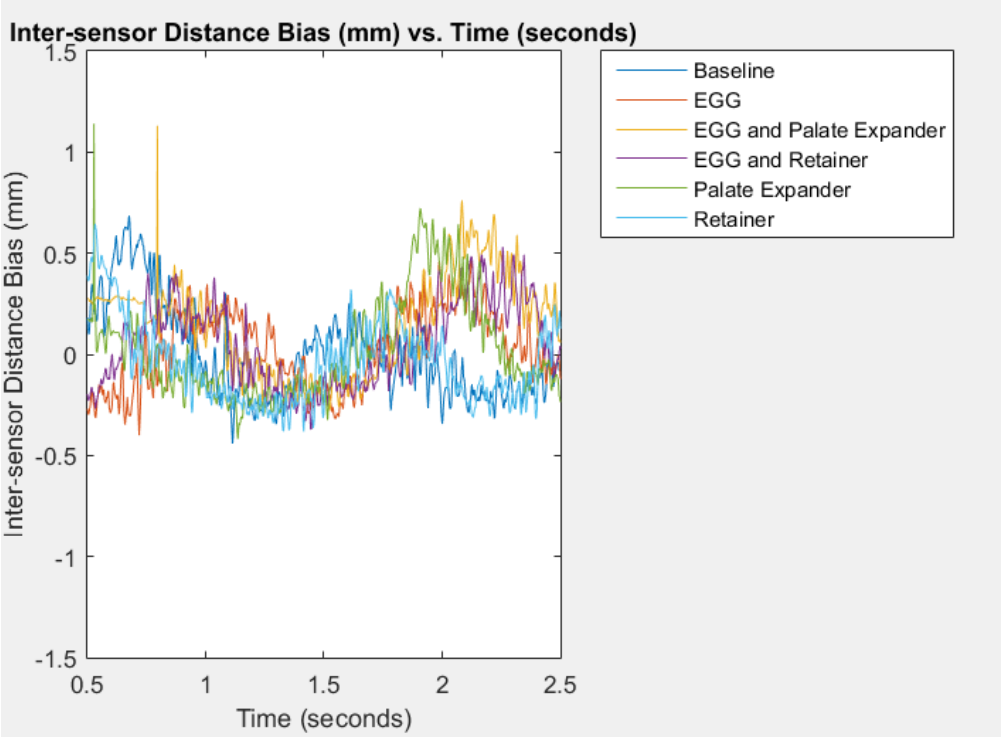

Figure 48 - Inter-sensor distance bias for sensors 2 and 3 in the non-ferrous orientation model

Table 49 - Comparison of average baseline inter-sensor distance with average inter-sensor distance of each interference trial for sensors 2 and 3 in the non-ferrous orientation model

Trial condition (outside)	Inter-sensor distance (mm)	Bias (mm)	% difference
Baseline	77.340	------	------
EGG	77.348	0.008	0.010
EGG and Retainer	77.489	0.148	0.192
EGG and Palate Expander	77.479	0.139	0.180
Retainer	77.356	0.016	0.021
Palate Expander	77.311	-0.029	-0.38

Table 50 - Maximum error for sensors 2 and 3 in the non-ferrous orientation model

	Bias (mm)	Standard deviation (mm)	Maximum error (mm)
Baseline	0	0.214	0.214
EGG	0.008	0.202	0.210
EGG and Retainer	0.148	0.312	0.460

EGG and Palate Expander	0.139	0.221	0.360
Retainer	0.016	0.208	0.224
Palate Expander	-0.029	0.257	-0.286

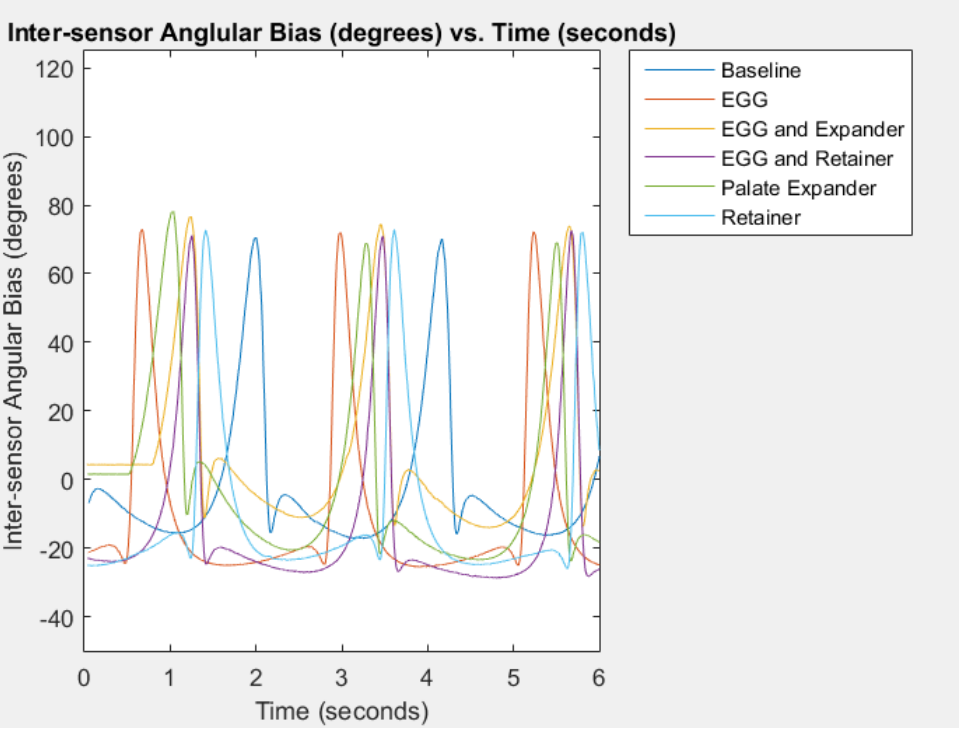

Figure 49 - Inter-sensor angular bias for sensors 2 and 3 in the non-ferrous orientation model

Table 51 - Inter-sensor angle bias present with different interference conditions

Trial condition	Average inter-sensor angle (°)	Bias (°)	% difference
Baseline	48.993	------	------
EGG	38.395	-10.598	-21.631
EGG and retainer	30.161	-19.832	-38.438
EGG and palate expander	52.728	3.735	7.624
Retainer	35.070	-13.922	-28.417
Palate expander	39.486	-9.506	-19.403

Table 52 - Maximum error of sensors 6 and 5 for the non-ferrous rotation model

Trial condition	Inter-sensor angular bias (°)	Standard deviation (°)	Maximum error (°)
Baseline	0	22.626	22.626
EGG	-10.598	25.574	-36.172
EGG and retainer	-19.832	24.295	-44.127
EGG and palate expander	3.735	24.022	27.757
Retainer	-13.922	25.680	-39.602
Palate expander	-9.506	24.557	-34.063

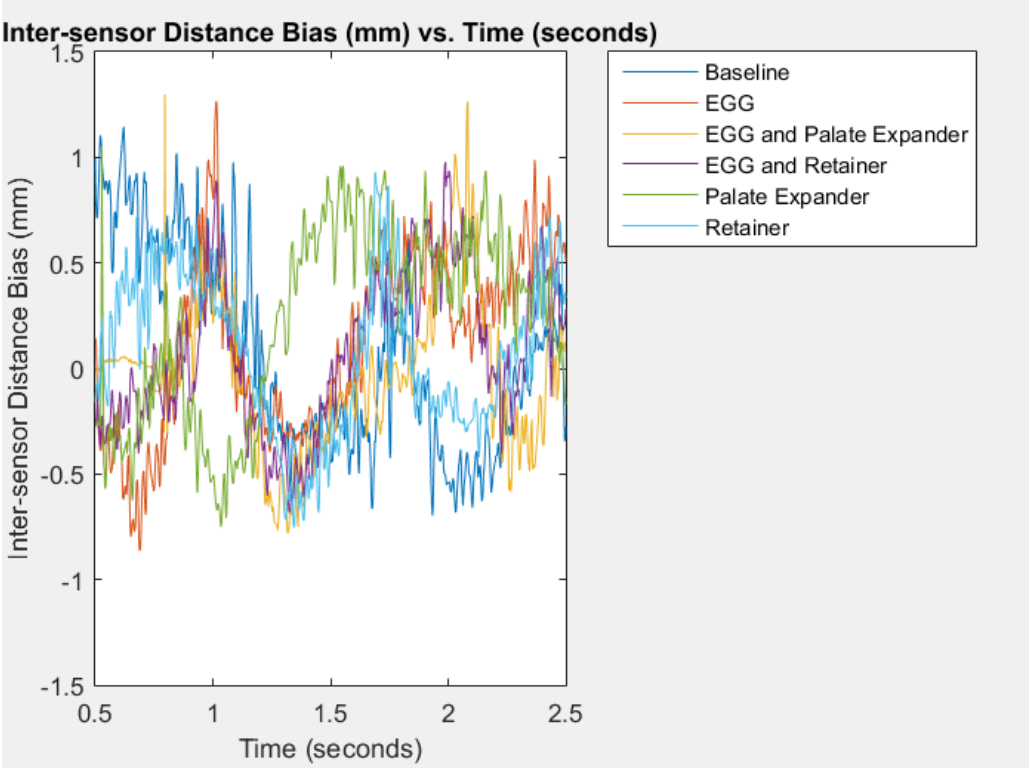

Figure 50 - Inter-sensor distance bias for sensors 1 and 3 in the non-ferrous orientation model

Table 53 - Comparison of average baseline inter-sensor distance with average inter-sensor distance of each interference trial for sensors 1 and 3 in the non-ferrous orientation model

Trial condition (outside)	Inter-sensor distance (mm)	Bias (mm)	% difference
Baseline	151.729	-------	------
EGG	151.789	0.060	0.040
EGG and Retainer	151.714	-0.015	-0.010

EGG and Palate Expander	151.667	-0.062	-0.041
Retainer	151.767	0.038	0.025
Palate Expander	151.818	0.089	0.059

Table 54 - Maximum error for sensors 1 and 3 in the non-ferrous orientation model

	Bias (mm)	Standard deviation (mm)	Maximum error (mm)
Baseline	0	0.401	0.401
EGG	0.060	0.362	0.422
EGG and Retainer	-0.015	0.293	-0.308
EGG and Palate Expander	-0.062	0.324	-0.386
Retainer	0.038	0.337	0.375
Palate Expander	0.089	0.476	0.565

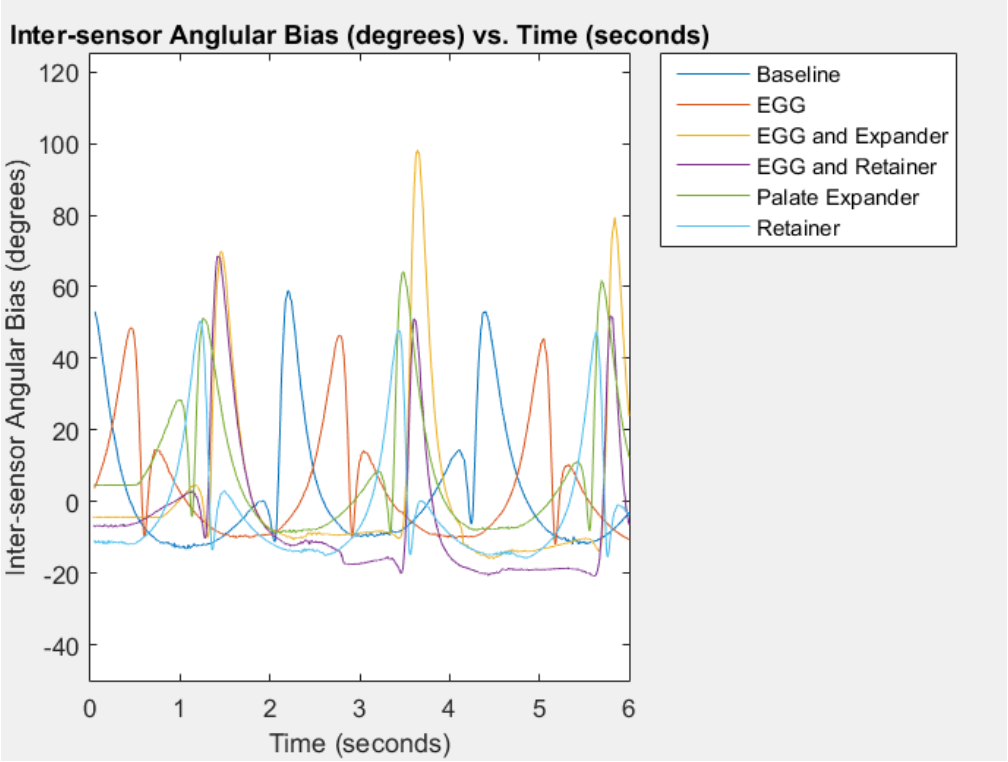

Figure 51 - Inter-sensor angular bias for sensors 1 and 3 in the non-ferrous orientation model

Table 55 - Inter-sensor angular bias present with different interference conditions

Trial condition	Average inter-sensor angle (°)	Bias (°)	% difference
Baseline	33.167	------	------
EGG	28.558	-4.609	-13.897
EGG and retainer	23.987	-9.181	-27.679
EGG and palate expander	34.258	1.090	3.288
Retainer	28.199	-4.968	-14.979
Palate expander	39.138	5.971	18.003

Table 56 - Maximum error of sensors 6 and 5 for the non-ferrous rotation model

Trial condition	Inter-sensor angular bias (°)	Standard deviation (°)	Maximum error (°)
Baseline	0	23.478	23.478
EGG	-4.609	16.022	-20.631
EGG and retainer	-9.181	19.823	-29.004
EGG and palate expander	1.090	24.570	25.660
Retainer	-4.968	15.489	-20.457
Palate expander	5.971	18.005	23.976